Article

SOURCE DATA | TRANSPARENT PROCESS | OPEN ACCESS

EMBO reports

Phosphorylation of β-catenin Ser60 by polo-like kinase 1 drives the completion of cytokinesis

Ji Eun Yu[1,2], Sun-Ok Kim[1], Jeong-Ah Hwang[3], Jin Tae Hong[2], Joonsung Hwang[1], Nak-Kyun Soung[1], Hyunjoo Cha-Molstad[1], Yong Tae Kwon[4], Bo Yeon Kim[1,5,*] & Kyung Ho Lee[1,**]

Abstract

β-Catenin is a multifunctional protein and participates in numerous processes required for embryonic development, cell proliferation, and homeostasis through various molecular interactions and signaling pathways. To date, however, there is no direct evidence that β-catenin contributes to cytokinesis. Here, we identify a novel p-S60 epitope on β-catenin generated by Plk1 kinase activity, which can be found at the actomyosin contractile ring of early telophase cells and at the midbody of late telophase cells. Depletion of β-catenin leads to cytokinesis-defective phenotypes, which eventually result in apoptotic cell death. In addition, phosphorylation of β-catenin Ser60 by Plk1 is essential for the recruitment of Ect2 to the midbody, activation of RhoA, and interaction between β-catenin, Plk1, and Ect2. Time-lapse image analysis confirmed the importance of β-catenin phospho-Ser60 in furrow ingression and the completion of cytokinesis. Taken together, we propose that phosphorylation of β-catenin Ser60 by Plk1 in cooperation with Ect2 is essential for the completion of cytokinesis. These findings may provide fundamental knowledge for the research of cytokinesis failure-derived human diseases.

Keywords cytokinesis; Ect2; Midbody; Plk1; β-Catenin p-S60
Subject Categories Cell Cycle; Post-translational Modifications & Proteolysis; Signal Transduction
DOI 10.15252/embr.202051503 | Received 10 August 2020 | Revised 31 August 2021 | Accepted 9 September 2021 | Published online 29 September 2021
EMBO Reports (2021) 22: e51503

Introduction

β-Catenin is an armadillo (ARM) repeat family protein and contributes to various fundamental cellular processes in animals. β-Catenin was discovered twice independently, as an E-cadherin-related cell adhesion molecule (Ozawa *et al*, 1989) and as a major component of canonical Wnt signaling (Weischaus & Riggleman, 1987; Riggleman *et al*, 1990). In canonical Wnt signaling, phosphorylation by upstream kinases is a key step in regulating β-catenin stabilization. Sequential phosphorylation of β-catenin Ser45 and Ser33/Ser37/Thr41 residues by casein kinase 1 alpha (CK1α) and glycogen synthase kinase 3 beta (GSK3β), respectively, leads to destabilization of β-catenin (Liu *et al*, 1999, 2002; Winston *et al*, 1999; Peifer & Polakis, 2000; Moon *et al*, 2002; Nelson & Nusse, 2004; Wu & He, 2006), whereas stimulation by the canonical Wnt ligand protects β-catenin against degradation and facilitates its nuclear accumulation, where β-catenin binds to lymphoid enhancing factor/T-cell factor (LEF/TCF) transcription factors and triggers canonical Wnt ligand-induced transcription (Behrens *et al*, 1996; Huber *et al*, 1996; Molenaar *et al*, 1996; Brunner *et al*, 1997; van de Wetering *et al*, 1997).

Through these various interactions, β-catenin contributes to Wnt-mediated transcription, chromatin remodeling, centrosomal maintenance/separation, epithelial–mesenchymal transition (EMT), and regulation of cell adhesion (Dierick & Bejsovec, 1999; Eastman & Grosschedl, 1999; Kaplan *et al*, 2004; Bahmanyar *et al*, 2008; Heuberger & Birchmeier, 2010; Yang *et al*, 2004; Conacci-Sorrell *et al*, 2003; Barrallo-Gimeno & Nieto, 2005; reviewed in Nelson & Nusse, 2004). Moreover, various Wnt signaling components, including β-catenin and Dishevelled, have been found in the centrosome, kinetochore, and mitotic spindle (Schlesinger *et al*, 1999; Bahmanyar *et al*, 2008; Kikuchi *et al*, 2010; Mbom *et al*, 2013; Kyun *et al*, 2020). Therefore, mitotic functions of Wnt signaling, including spindle orientation, centrosome separation, mitotic cell division, and chromosome segregation, have all been proposed (Kaplan *et al*, 2004; Walston *et al*, 2004; Hadjihannas *et al*, 2006; Aoki *et al*, 2007; Bahmanyar *et al*, 2008; Kikuchi *et al*, 2010). While there is no direct evidence for involvement in cytokinesis, numerous reports have identified β-catenin mutations or overexpression in colorectal, breast, prostate, lung, liver, ovarian, and endometrial cancers (Bienz & Clevers, 2000; Peifer & Polakis, 2000; Behrens, 2005; reviewed in Kim & Jeong, 2019), and abnormal cytokinesis is implicated in tumorigenesis. Here we present a potential explanation for tumorigenesis caused by aberrant β-catenin function in cytokinesis.

Cytokinesis is the final stage of cell division, producing two daughter cells from one mother cell. The cellular mechanisms and molecular

1 Anticancer Agent Research Center, Korea Research Institute of Bioscience and Biotechnology (KRIBB), Ochang, Chungbuk, Korea
2 Department of Drug Discovery and Development, College of Pharmacy, Chungbuk National University, Cheongju, Korea
3 Department of Physiology, Research Institute of Medical Sciences, College of Medicine, Chungnam National University, Daejeon, Korea
4 Protein Metabolism Medical Research Center and Department of Biomedical Sciences, College of Medicine, Seoul National University, Seoul, Korea
5 Department of Biomolecular Science, University of Science and Technology, Daejeon, Korea
*Corresponding author. Tel: +82 43 240 6163; Fax: +82 43 240 6259; E-mail: bykim@kribb.re.kr
**Corresponding author. Tel: +82 43 240 6256; Fax: +82 43 240 6259; E-mail: leekh@kribb.re.kr

© 2021 The Authors. Published under the terms of the CC BY NC ND 4.0 license

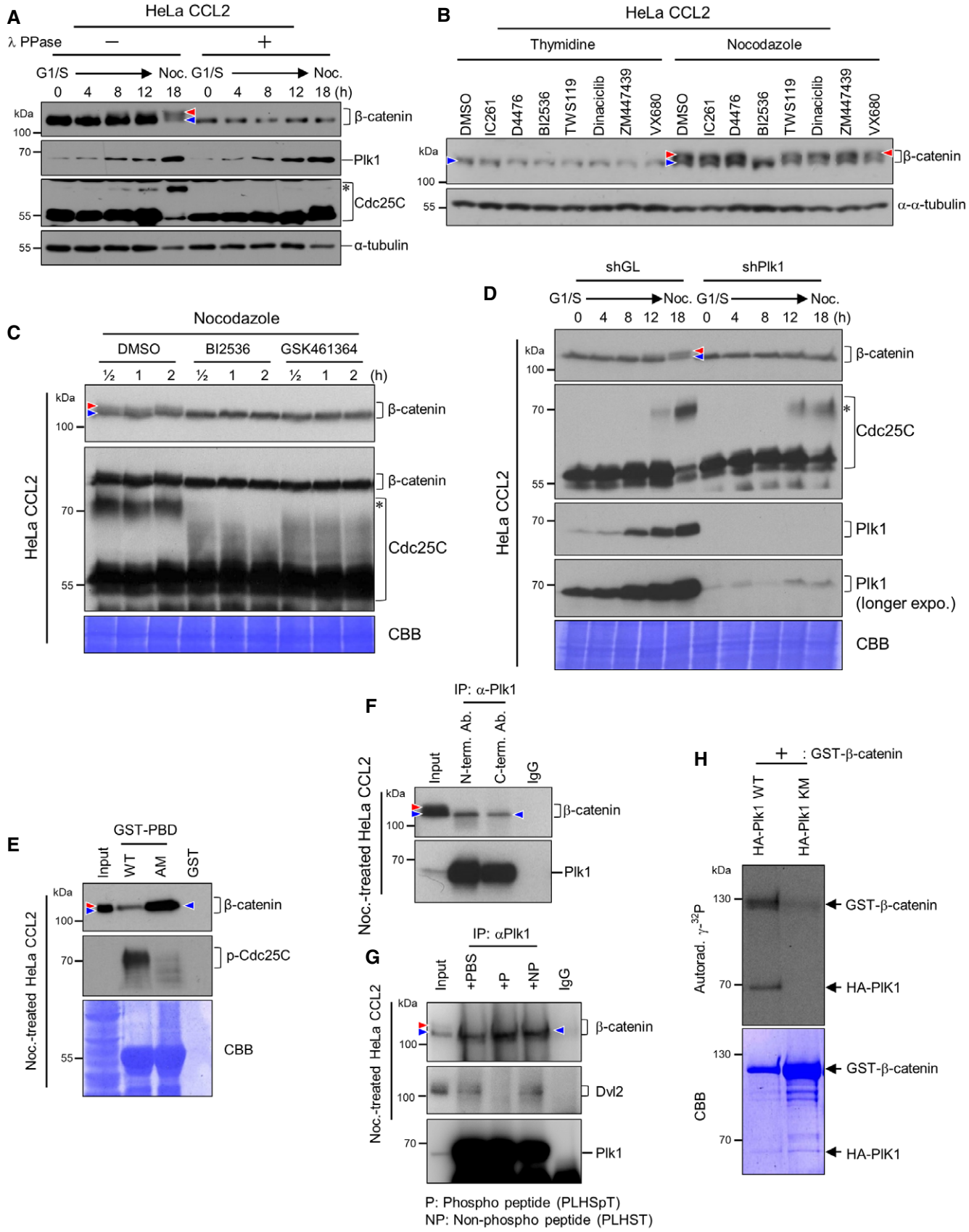

Figure 1.

© 2021 The Authors

Figure 1. β-Catenin is hyperphosphorylated by Plk1 during the mitotic phase.

A β-Catenin is hyperphosphorylated during the mitotic phase. HeLa CCL2 cells were synchronized at the G1/S phase using a double thymidine block and released using medium containing 200 ng/mL nocodazole (Noc.). Cells were harvested at the indicated time points and treated with (+) or without (−) λ-phosphatase (λ-PPase). The resulting cell lysates were used for immunoblot analysis. Hyperphosphorylated β-catenin (red arrowhead) was distinguished from non-/less-phosphorylated β-catenin (blue arrowhead) by slower migration during SDS–PAGE. Asterisk indicates the phosphorylated form of Cdc25C.

B Treatment with the Plk1 kinase inhibitor BI 2536 converts the slower-migrating β-catenin form to the faster-migrating β-catenin form. Thymidine (S phase) or nocodazole (M-phase)-arrested HeLa CCL2 cells were treated with the indicated kinase inhibitors to inhibit CK1δ/ϵ (IC261), CK1δ (D4476), Plk1 (BI2536), GSK3β (TWS119), CDK2/5/1/9 (Dinaciclib), Aurora kinase A/B (ZM447439), or Aurora kinase A (VX680). The resulting cell lysates were used for immunoblot analyses. Only BI2536 converted slower-migrating (red arrowhead) to faster-migrating β-catenin (blue arrowhead).

C Plk1-specific inhibitors rapidly abolished the phosphorylated form of β-catenin (red arrowhead). Nocodazole-arrested HeLa CCL2 cells were treated with two different Plk1 inhibitors, BI2536 and GSK461364, for the indicated times. Asterisk indicates the phosphorylated form of Cdc25C. BI2536 or GSK461364 treatment converted slower-migrating (red arrowhead) to faster-migrating β-catenin (blue arrowhead).

D Asynchronously growing HeLa CCL2 cells were silenced for either control luciferase (shGL) or Plk1 (shPlk1) using lentivirus-based shRNA infection. The resulting cells were synchronized using a double thymidine block and released using medium containing 200 ng/ml nocodazole (Noc.). Cells were harvested at the indicated time points and used for immunoblot analyses. Asterisk indicates the phosphorylated form of Cdc25C. Hyperphosphorylated β-catenin (red arrowhead) was distinguished from non-/less-phosphorylated β-catenin (blue arrowhead) by slower migration during SDS–PAGE.

E β-Catenin interacts with Plk1 PBD in a phosphorylation-independent manner. Total cell lysates from nocodazole (Noc.)-treated HeLa CCL2 cells were incubated and pull downed with bacterially purified/bead-associated GST–Plk1 PBD wild-type (WT), GST–Plk1 PBD H538A and K540M mutant (AM), or GST only. The resulting precipitates were subjected to immunoblot analyses. Hyperphosphorylated β-catenin (red arrowhead) was distinguished from non-/less-phosphorylated β-catenin (blue arrowhead) by slower migration during SDS–PAGE.

F Total cell lysates from nocodazole (Noc.)-treated HeLa CCL2 cells were immunoprecipitated with two different Plk1 antibodies. Each antibody (gifted from Kyung S. Lee, NIH/NCI) recognized either Plk1 N terminus (N-term. Ab.) or C terminus (C-term. Ab.). The resulting precipitates were subjected to immunoblot analysis. Hyperphosphorylated β-catenin (red arrowhead) was distinguished from non-/less-phosphorylated β-catenin (blue arrowhead) by slower migration during SDS–PAGE.

G Lysates from nocodazole (Noc.)-treated HeLa CCL2 cells were mixed with either control (phosphate-buffered saline only, +PBS), 10 μg/ml of high-affinity Plk1 PBD-binding phosphopeptide (PLHSpT, +P), or 10 μg/ml of non-phosphopeptide (PLHST, +NP). The resulting cell lysates were immunoprecipitated with anti-Plk1 antibody. Precipitates were subjected to immunoblot analysis. Immunoblotting with anti-Dvl2 antibody represents a positive control of phosphopeptide (PLHSpT, +P) competition for Plk1 binding. Hyperphosphorylated β-catenin (red arrowhead) was distinguished from non-/less-phosphorylated β-catenin (blue arrowhead) by slower migration during SDS–PAGE.

H β-Catenin is directly phosphorylated by Plk1. Bacterially purified full-length GST–β-catenin was incubated with either HA–Plk1 wild-type (WT) or HA–Plk1 kinase defective mutant K82M (KM) purified from insect cells in the presence of [γ-^{32}P] ATP. Incorporation of γ-^{32}P into GST–β-catenin was confirmed by SDS–PAGE followed by autoradiography analysis.

Source data are available online for this figure.

components of cytokinesis vary among organisms. Preparation for animal cell cytokinesis begins in interphase and progresses rapidly concomitant with the morphological changes of mitosis, including cell rounding, spindle orientation, cell elongation, cortical stabilization, symmetric furrowing, furrow ingression, bridge stabilization, abscission, and midbody remnant clearance (reviewed in Eggert *et al*, 2006; Fededa & Gerlich, 2012). Cytokinesis in animal cells is generally defined from the central spindle assembly of anaphase to the abscission of telophase. Since cytokinesis is a critical step for proper maintenance and transmission of genetic material to offspring, cytokinesis defects produce aneuploid cells, which are a major cause of human solid tumors (reviewed extensively elsewhere; Weaver & Cleveland, 2007; Green *et al*, 2012; Duijf *et al*, 2013; Lens & Medema, 2019).

Complex cooperation among the cytoskeleton, cell membrane components, and regulatory proteins such as kinases is required for proper cytokinesis. Separation of chromatid pairs to the opposite spindle pole during anaphase induces cleavage furrow ingression. At the molecular level, this requires activation of the small GTPase RhoA at the equatorial cell cortex by the Rho guanine nucleotide exchange factor (Rho-GEF) Ect2, which in turn promotes contractile actomyosin ring assembly by actin filament polymerization and myosin II activation (Bement *et al*, 2005; Yuce *et al*, 2005; Odell & Foe, 2008). Migration of Ect2 toward the equatorial complex is initiated by phosphorylation of CYK-4 by polo-like kinase 1 (Plk1), which promotes Ect2−CYK-4 complex formation at the central spindle, while subsequent inactivation of cyclin-dependent kinase 1 (CDK1) induces migration of Ect2 toward the equatorial cell cortex (Yuce *et al*, 2005; Zhao & Fang, 2005; Nishimura & Yonemura, 2006; Birkenfeld *et al*, 2007; Petronczki *et al*, 2007; Wolfe *et al*, 2009; Su *et al*, 2011). Plk1 is critical for early mitosis events such as mitotic entry, centrosome maturation, and kinetochore attachment (reviewed extensively elsewhere; Barr *et al*, 2004; Petronczki *et al*, 2008; Kishi *et al*, 2009). In addition, Plk1 is also implicated in the late stage of mitosis and the non-mitotic phase of the cell cycle (Brennan *et al*, 2007; Burkard *et al*, 2007; Petronczki *et al*, 2007; Santamaria *et al*, 2007; Lee *et al*, 2012, 2017, 2018). For instance, Plk1 activity is indispensable for the proper localization of centralspindlin subunits such as Mklp1 and HsCyk-4 as well as for Ect2 recruitment to the midbody (Brennan *et al*, 2007; Burkard *et al*, 2007; Petronczki *et al*, 2007; Santamaria *et al*, 2007), but the precise mechanism by which Plk1 activity regulates cytokinesis remains largely unknown.

More than 20 phosphorylation sites have been identified in β-catenin (reviewed in Valenta *et al*, 2012). This study identifies a new phosphorylation site mediating a novel cytokinetic function of β-catenin in coordination with Plk1 and Ect2 that provides a fundamental knowledge for cancer research. Since cytokinesis defects lead to a variety of human cancers (reviewed extensively elsewhere; Kim & Jeong, 2019; Lens & Medema, 2019), this newly described function of β-catenin in cytokinesis may provide the fundamental knowledge that is vital for cancer research.

Results

Phosphorylation of β-catenin by Plk1 during mitosis

We monitored β-catenin protein modifications such as phosphorylation during synchronized cell cycle progression by electrophoresis

© 2021 The Authors

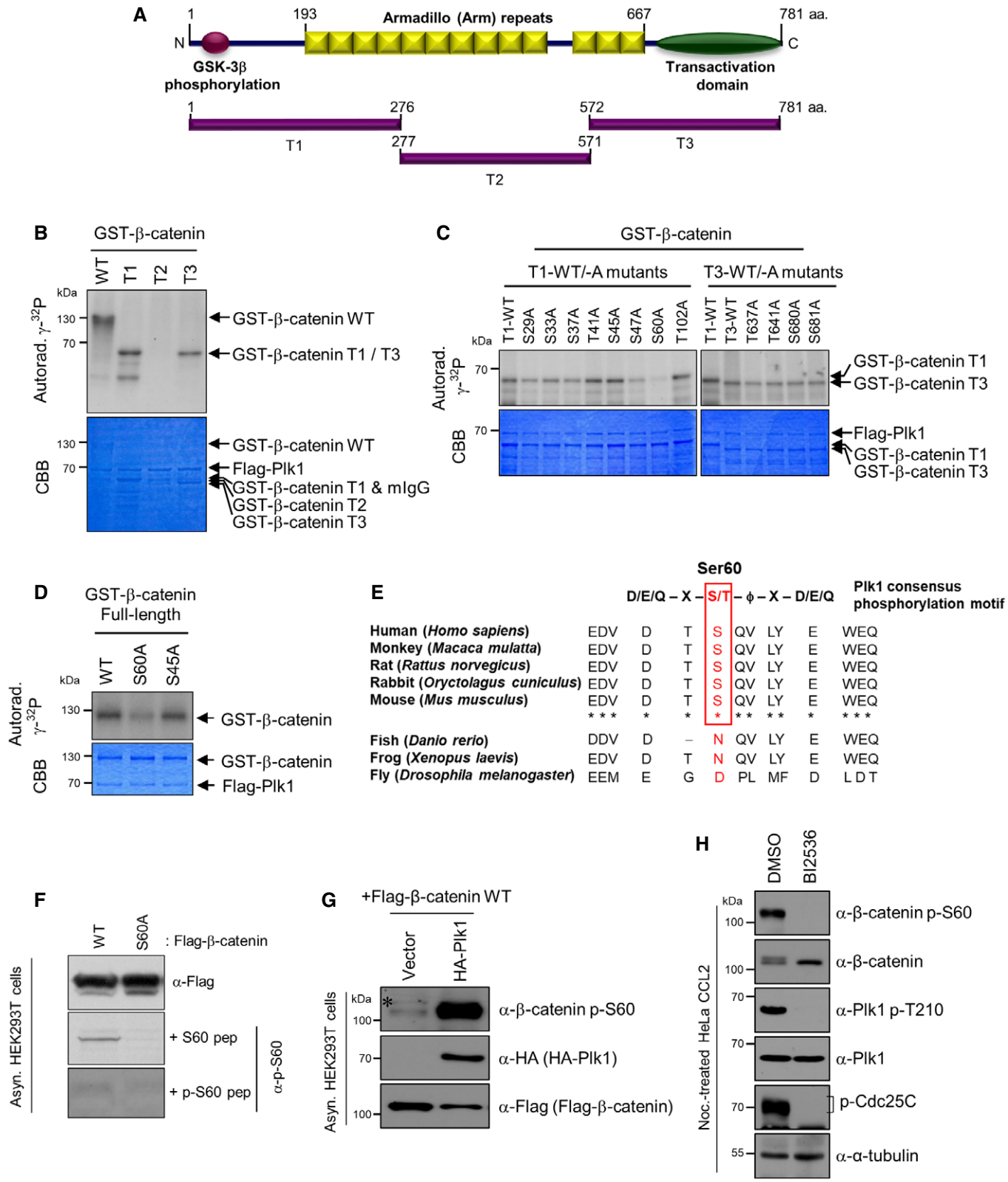

Figure 2.

© 2021 The Authors

Figure 2. Phosphorylation of β-catenin Ser60 residue by Plk1.

A Schematic diagram of the β-catenin domain structure and truncation mutants used in this study. The amino acid positions, truncation mutant names, and domain names are indicated.

B Bacterially produced full-length GST–β-catenin and truncation mutant proteins were purified and reacted with Flag–Plk1 WT produced from mammalian cells in the presence of [γ-^{32}P]ATP. Incorporation of ^{32}P into GST–β-catenin WT and truncation mutants was confirmed by SDS–PAGE followed by autoradiography.

C Bacterially produced β-catenin T1 WT, T3 WT, and corresponding alanine ("A") mutants were purified and reacted with Flag–Plk1 WT in the presence of [γ-^{32}P]ATP. Incorporation of ^{32}P onto each "A" mutant of β-catenin was confirmed by SDS–PAGE followed by autoradiography analysis.

D Bacterially produced full-length β-catenin WT and alanine ("A") substitution mutants were purified and reacted with Flag–Plk1 WT produced from mammalian cells in the presence of [γ-^{32}P]ATP. Incorporation of ^{32}P into each "A" mutant or full-length WT β-catenin was confirmed by SDS–PAGE followed by autoradiography analysis.

E The Ser60 residue of β-catenin is highly conserved among various species. Plk1 consensus phosphorylation sequence ([D/E/Q]-X-[pS/pT]-ϕ-X-[D/E/Q]) was shown. Ser60 is marked in red. X, any amino acid residue; ϕ, hydrophobic residue.

F A phospho-specific antibody against the β-catenin p-S60 epitope was generated and validated. Asynchronously growing HEK293T cells transfected with either Flag–β-catenin WT or S60A mutant (S60A) were harvested and immunoblotted using an anti-β-catenin p-S60 specific antibody. To confirm the specificity, either non-phospho-Ser60 peptide (+ S60 pep) or phospho-S60 peptide (+ p-S60 pep) was added to antibody solution prior to membrane incubation.

G Asynchronously growing HEK293T cells co-transfected with Flag–β-catenin WT and either HA–Plk1 WT or control (vector only) were harvested and subjected to immunoblot analysis using the indicated antibodies. Asterisk, a nonspecific cross-reacting band.

H HeLa CCL2 cells were treated for 18 h with 200 ng/ml nocodazole followed by treatment with either DMSO (control) or BI 2536 for an additional 1 h. The resulting cells were lysed with 2× Laemmli SDS sample buffer and used for immunoblot analysis with the indicated antibodies.

Source data are available online for this figure.

to identify potentially novel mitotic functions. HeLa CCL2 cells were synchronized at the G1/S phase using double thymidine block and then released at different time points or arrested at mitosis via treatment with nocodazole. β-Catenin protein was detected by SDS–PAGE as a doublet band during the mitotic phase (Fig 1A), suggesting novel post-translational modifications during mitosis. Treatment of β-catenin isolated from mitotic cells with lambda protein phosphatase (λ PPase) abolished the slower-migrating β-catenin band (Fig 1A), suggesting hyperphosphorylation of β-catenin by kinase(s) during mitosis.

To identify the kinase(s) responsible, HeLa CCL2 cells were treated with either thymidine to arrest the cell cycle during S phase or nocodazole to arrest cells in M-phase prior to treatment with specific kinase inhibitors. Among these kinase inhibitors, the Plk1 inhibitor BI 2536 abolished the slow-migrating phosphorylated β-catenin in mitotic cells (Fig 1B). To confirm this result, nocodazole-arrested HeLa CCL2 cells were treated with BI 2536 or another Plk1 inhibitor, GSK461364. Phosphorylation of β-catenin was eliminated by treatment with both Plk1 inhibitors, even after only 30 min of treatment (Fig 1C). Hyperphosphorylation of β-catenin by Plk1 during mitosis was further supported by knockdown experiments, as the slower-migrating band completely disappeared in Plk1 knockdown cells while the β-catenin doublet remained in mitotic control luciferase knockdown cells (Fig 1D). Based on these results, we speculated that β-catenin is a substrate for Plk1. For many Plk1 substrates, binding and subsequent phosphorylation require a priming phosphorylation event at another residue. Here, we demonstrate an interaction between Plk1 and β-catenin by immunoprecipitation and GST pull-down assay (Appendix Fig S1A–C). The precise physical relationship between β-catenin and Plk1 was investigated by performing a pull-down assay using a fusion construct of GST and the Plk1 polo-box domain (Plk1 PBD). Unexpectedly, we found phosphorylation-independent binding of β-catenin to Plk1 PBD. β-Catenin bound to GST-PBD H538A/K540M (AM) mutant that is defective in phosphorylation-dependent binding (Elia *et al*, 2003) as well as GST-PBD wild type (WT) (Fig 1E). This phosphorylation-independent binding was confirmed twice by immunoprecipitation and peptide competition analyses. Immunoprecipitation using two different Plk1 antibodies revealed that the faster-migrating (non/less-phosphorylated) endogenous β-catenin bound to Plk1 during the mitotic phase (Fig 1F). Moreover, addition of the previously characterized Plk1 PBD-binding phosphopeptide PLHSpT (Yun *et al*, 2009) diminished the interaction between Plk1 and Dvl2 but did not alter the binding between Plk1 and β-catenin compared to the control non-phosphopeptide PLHST (Fig 1G). Although β-catenin bound Plk1 in a phosphorylation-independent manner, it was also phosphorylated by Plk1 as indicated by an *in vitro* kinase assay (Fig 1H). On the basis of these results, the phosphorylation of β-catenin by Plk1 may not require priming phosphorylation by other kinases, but as these results were obtained from *in vitro* experiments, more detailed experiments are needed to assess whether Plk1 phosphorylates β-catenin in the absence of priming phosphorylation.

Plk1 phosphorylates the Ser60 residue of β-catenin

We next aimed to identify the specific Plk1 phosphorylation site(s) of β-catenin. To this end, three GST-fused β-catenin truncation mutant constructs (T1, T2, and T3) (Fig 2A) were generated, expressed in bacteria, purified, and reacted with Flag-Plk1 WT purified from mammalian cells. *In vitro* kinase assays revealed that the β-catenin T1 region encompassing amino acids 1–276 and the T3 region encompassing amino acids 572–781 were phosphorylated by Plk1 while the T2 region (amino acids 277–571) was not (Fig 2B). Based on these findings, we attempted to identify specific Plk1 phosphorylation sites of β-catenin in the T1 and T3 mutants.

Serine and threonine residues within the consensus phosphorylation motif of Plk1 (D/E/Q-X-S/T-ϕ-X-D/E/Q; X, any amino acid; ϕ, hydrophobic residue) (Nakajima *et al*, 2003; Barr *et al*, 2004) in T1 and T3 mutants were selected as potential novel β-catenin phosphorylation sites as well as previously described β-catenin phosphorylation sites. Candidate Ser/Thr residues were mutated to alanine in the T1 and T3 mutants of β-catenin and purified GST-fused β-catenin alanine ("A") mutants were reacted with Flag–Plk1 WT purified from mammalian cells. Among the 12 candidate sites, only the Ser60 mutation (S60A) reduced the phosphorylation signal in response to Plk1 activity compared to T1 WT (Fig 2C). In accord with this observation, phosphorylation of full-length β-catenin S60A

© 2021 The Authors

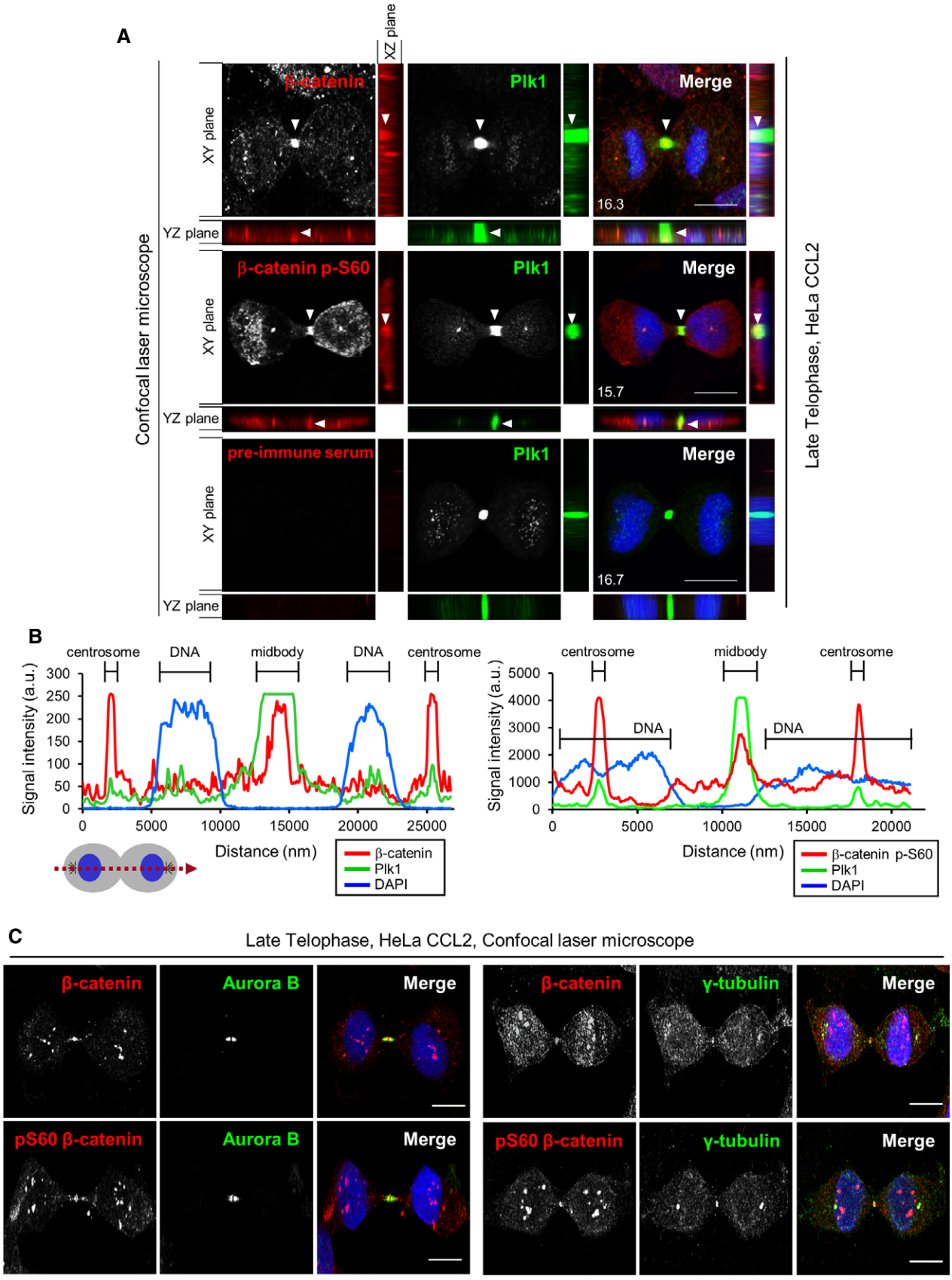

Figure 3.

© 2021 The Authors

Figure 3. Midbody localization of β-catenin p-S60 and Plk1 in telophase HeLa CCL2 cells.

A Asynchronously growing HeLa CCL2 cells were immunostained with the indicated antibodies after extraction using 0.2% Triton X-100. The resulting samples were observed using a confocal laser microscope (Zeiss LSM 700). Immunostaining with pre-immune serum in (A) represents the negative control for immunoreactivity. Scale bars, 10 μm. The value of the relative neck thickness is shown in the lower left corner of the merged images. The relative thickness of the neck was calculated as in Appendix Fig S6A.

B Intercentrosomal (centrosome-to-centrosome) linear signal profiles of β-catenin/Plk1 (left panel) and β-catenin p-S60/Plk1 (right panel) from the XY plane of the immunostained cells in (A).

C Asynchronously growing HeLa CCL2 cells were immunostained with the indicated antibodies as described in (A), and the midbody localization of β-catenin/β-catenin p-S60 in late telophase cells was observed using a confocal laser microscope (Zeiss LSM 700). Scale bars, 10 μm. All immunofluorescence images and linear signal profiles show representative data of more than 50 telophase cells obtained from three independent experiments (A, B). All images show representative data of more than 50 late telophase cells obtained from three independent experiments (C).

mutant was dramatically reduced compared to the WT or S45A (CK1α phosphorylation site) β-catenin mutant (Fig 2D). Conservation of Ser60 in β-catenin among various species also highlights the importance of this phosphorylation site (Fig 2E). Additionally, *in vivo* phosphorylation of S60 by Plk1 was confirmed by immunoblot analysis using a phospho-specific antibody generated against the β-catenin p-S60 epitope (Fig 2F).

To confirm that Plk1 activity is responsible for phosphorylation of β-catenin Ser60, HeLa cells were transfected with HA–Plk1 and the cell lysates immunoblotted with the anti-p-S60-specific antibody. Plk1 expression markedly induced or increased β-catenin Ser60 phosphorylation compared to control vector expression (Fig 2G), while pharmaceutical inhibition of Plk1 using BI 2536 reduced expression of the β-catenin p-S60 epitope (Fig 2H).

Midbody-localized β-catenin p-S60 is involved in cytokinesis

To identify the function of β-catenin p-S60, we first investigated the subcellular localization of total β-catenin and β-catenin p-S60 during cell cycle progression by immunofluorescence. Surprisingly, immunoreactivity of both forms was observed at the midbody in late telophase cells. Moreover, the midbody β-catenin signal clearly co-localized with Plk1 signals in late telophase HeLa CCL2 cells (Fig 3A and B) as well as in NRK, MRC-5, 267B1, and MEF cells (Appendix Fig S2A). In late-anaphase cells, Plk1 was localized to a band of spindle microtubules in the central spindle, and β-catenin was enriched in the equatorial cortex. As the cell cycle progressed from late anaphase to early telophase, both Plk1 and β-catenin were enriched in a compact manner at the cell midbody (Appendix Fig S2B). Immunostaining with additional cellular marker proteins also revealed the specific localization of β-catenin at the midzone/midbody (Appendix Fig S2C). We co-immunostained for β-catenin together with the membrane marker proteins E-cadherin and Na^+/K^+ATPase. The staining pattern of β-catenin differed from that of the membrane marker proteins: E-cadherin and Na^+/K^+ATPase were both localized over the whole cell, and a small fraction of those proteins was localized to the midzone/midbody. However, β-catenin was enriched prominently at the midzone/midbody. In addition, we found that the endogenous α-tubulin signal was masked at the dark zone whereas the endogenous β-catenin and pS60 signals accumulated at the central dark zone of the midbody (Appendix Fig S2C).

To verify these findings, the signal of total β-catenin/β-catenin p-S60 was compared to that of midbody marker proteins such as Aurora B or γ-tubulin in more spreading late telophase cells. During late telophase, total β-catenin/β-catenin p-S60 overlapped with γ-tubulin at the midbody core. In addition, signals of total β-catenin or β-catenin p-S60 were observed between Aurora B signals localized at the flanking regions of the midbody in late telophase cells (Fig 3C). These localizations were accurately analyzed in early telophase cells using a super-resolution confocal laser scanning microscope. Early telophase cells immunostained with anti-β-catenin/anti-Plk1/anti-β-catenin p-S60/anti-F-actin revealed that the merged signal of β-catenin p-S60 and Plk1 was localized at the center of the total β-catenin signal, and F-actin surrounded total β-catenin signal in contractile ring region (Fig 4A and B). To further confirm this observation, we measured the width of β-catenin/β-catenin p-S60 in the neck of early telophase cells (Fig 4C). The immunofluorescence signal of total β-catenin covered more than 80% of the neck, whereas β-catenin p-S60 covered only about 30% of the neck in early telophase cells. Therefore, we speculate that β-catenin is one of the contractile ring components, and the phosphorylation of β-catenin S60 by Plk1 may induce contractility during early telophase.

These data suggest an essential function of β-catenin in cytokinesis. To test this hypothesis directly, endogenous β-catenin was depleted in cell lines stably expressing WT, S60A, S60D β-catenin, or vector-only using a β-catenin-knockdown lentivirus (shβ-catenin) (Fig 5A). Downregulation of β-catenin or expression of S60A led to cytokinesis-defective phenotypes, such as an increase in the number of cells with multinucleated phenotypes compared to the control cells (shGL cells). Conversely, expression of either S60D or WT β-catenin reduced cytokinesis-defective phenotypes (Fig 5B and C). The depletion of β-catenin resulted in a more than threefold increase in the number of multinucleated cells compared to the control (shGL). Stable expression of the S60A mutant in endogenous β-catenin-depleted cells yielded cytokinesis-defective phenotypes similar to β-catenin-depleted cells. In contrast, stable expression of WT or S60D mutant β-catenin resulted in cytokinesis-defective phenotypes similar to control luciferase knockdown cells (shGL) (Fig 5C). These cytokinesis-defective phenotypes induced by mutation of the β-catenin Ser60 residue were also confirmed by overexpression (Appendix Fig S3A and B). In line with these observation, fluorescence-activated cell sorting (FACS) demonstrated a marked increase in > 4N cells and a moderate increase in sub-G1 cells induced by β-catenin knockdown compared with control -knockdown cells (Fig 5D). The increase in the sub-G1 population by β-catenin knockdown, indicative of apoptosis, was further confirmed by TUNEL analysis (Appendix Fig S4A–C).

We next investigated whether defective cytokinesis was caused by the reduction of β-catenin p-Ser60 epitope by monitoring live cells using time-lapse imaging. Since time-lapse images for live-cell assays were observed in the culture dishes at low magnification, the

© 2021 The Authors

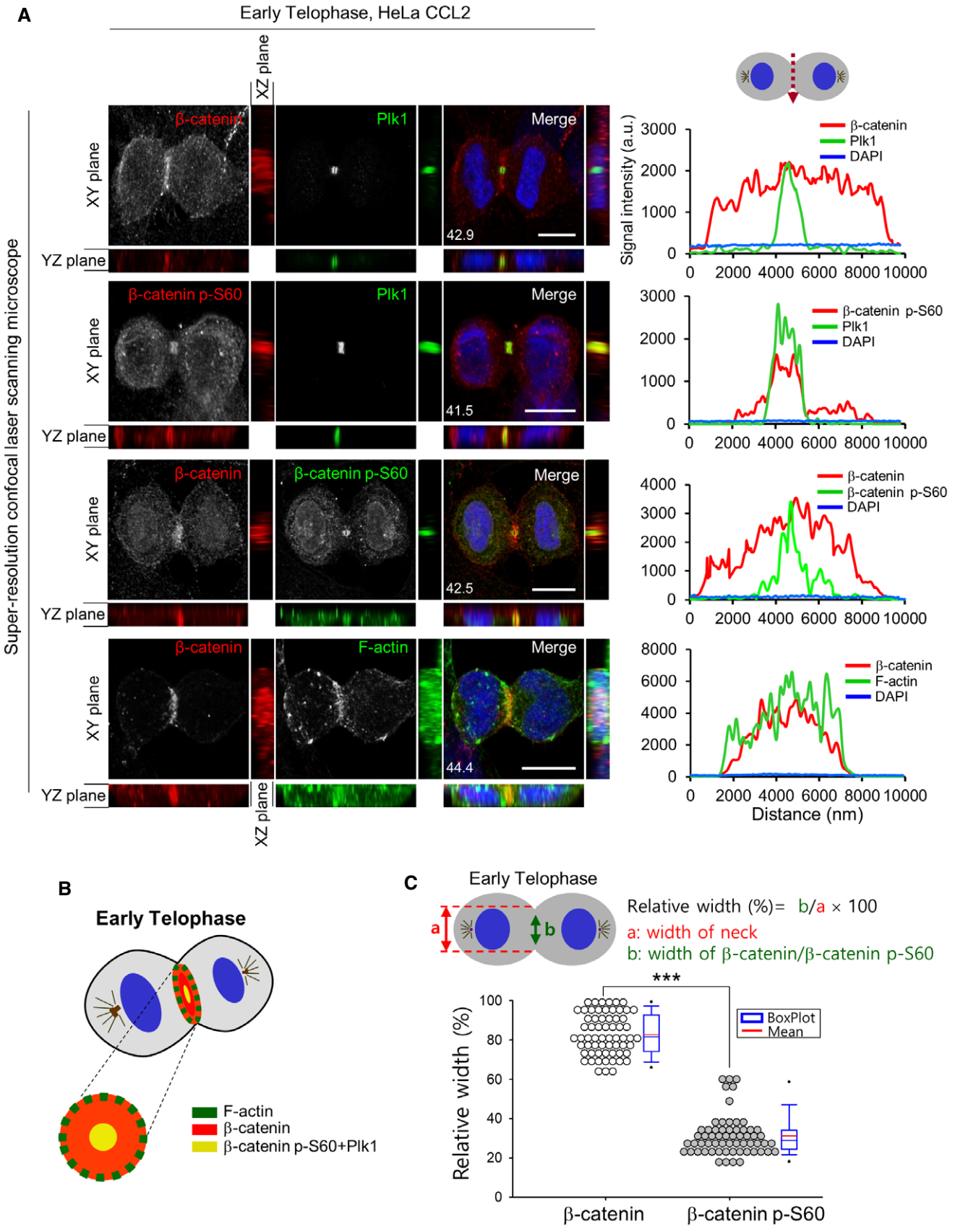

Figure 4.

© 2021 The Authors

Figure 4. β-Catenin p-S60 and Plk1 were surrounded by actomyosin contractile ring in early telophase cells.

A Asynchronously growing HeLa CCL2 cells were immunostained with the indicated antibodies, and early telophase cells were observed using a super-resolution confocal laser scanning microscope (LSM-880 with Airyscan) (left panel). Scale bars, 10 μm. Linear signal profiles of β-catenin/Plk1/β-catenin p-S60/F-actin in the contractile ring region from the XY plane of immunostained early telophase cells (right panel). All immunofluorescence images and linear signal profiles show representative data of more than 50 telophase cells obtained from three independent experiments. The value of the relative neck thickness is shown in the lower left corner of the merged images (A).

B Schematic diagram for the proposed localization of β-catenin/Plk1/β-catenin p-S60/F-actin in the contractile ring region from early telophase cells in (A).

C The width of the neck/β-catenin/β-catenin p-S60 from Fig 4A sample was measured (upper panel), and the relative width (%) was marked in the graph. A dot density graph with a box plot shows the relative width in early telophase cells. Approximately 60 cells from three independent experiments were measured. ***$P < 0.001$ (unpaired two-tailed *t*-test) The box plot represents: central blue band, median; box, interquartile range; upper whisker, maximum observation below upper fence; lower whisker, minimum observation above lower fence; dot, outlier.

proper subcellular localizations of fluorescence-tagged β-catenin constructs were first confirmed using immunofluorescence under high magnification (Fig 5E left panel, Appendix Fig S5A and B). The majority of the telophase cells showed midbody localizing GFP−β-catenin WT and GFP-β-catenin S60D. However, the phosphorylation-deficient mutant GFP−β-catenin S60A was not efficiently localized at the midbody compared to other constructs (Appendix Fig S5A and B). HEK 293T cells were co-transfected with histone H2B–mCherry and either GFP–β-catenin WT or S60A mutant. They were allowed to progress through mitosis; this was tracked using live-cell imaging, and the images were used for further analyses. Cells expressing WT β-catenin showed almost complete cleavage furrow ingression and cytokinesis. However, 52% of the cells transfected with S60A β-catenin were unable to complete furrow ingression. Some of the S60A-expressing cells showed no cleavage furrow ingression (30%) or cleavage furrow regression (22%), and eventual formation of multinucleated cells (Fig 5E and F, Movies EV1–EV3). These results indicate that phosphorylation of β-catenin at the Ser60 residue by Plk1 is critical for completion of cytokinesis.

β-Catenin mediates the interaction between Plk1 and Ect2 during mitotic progression

It was previously reported that the Rho-GEF Ect2 is activated by Plk1 and then interacts with the Rho GTPase RhoA to trigger formation of the contractile ring for cleavage furrow ingression (Niiya *et al*, 2006; Brennan *et al*, 2007; Burkard *et al*, 2007; Petronczki *et al*, 2007; Santamaria *et al*, 2007). Therefore, we aimed to identify a functional link between Plk1, β-catenin, and Ect2 in telophase cells. Immunostaining revealed that endogenous total β-catenin and β-catenin p-S60 were co-localized with endogenous Ect2 at the midbody during telophase (Fig 6A and B). Further, immunoprecipitation analysis suggested a physical interaction between endogenous β-catenin and HA−Ect2 (a gift from Adrienne Cox, University of North Carolina, NC) in asynchronously growing HeLa CCL2 cells (Fig 6C). Moreover, the interaction between HA−Ect2 and β-catenin was markedly higher in the mitotic phase compared to interphase. HeLa cells co-transfected with HA–Ect2 and GFP–β-catenin were synchronized at the G1/S phase using double thymidine block and released using nocodazole-containing medium at the indicated time points. HA–Ect2 was then immunoprecipitated using cell lysate samples from each time point and co-immunoprecipitated GFP−β-catenin was determined by immunoblot analysis. Results revealed that the interaction between both proteins was greatly increased 18 h after G1/S release using nocodazole-containing medium (Fig 6D). Therefore, we conclude that Ect2 and β-catenin preferentially interact during the mitotic phase.

To investigate whether β-catenin affects the interaction between Plk1 and Ect2, β-Catenin was depleted using an shRNA viral system in HeLa CCL2 cells co-expressing HA–Ect2 and Flag–Plk1, and immunoprecipitation was performed during telophase (6 h release after 18 h nocodazole treatment). Immunoprecipitation analysis indicated that the interaction between Flag–Plk1 and HA–Ect2 was almost completely eliminated by depletion of β-catenin (Fig 6E). Reciprocal immunoprecipitation analysis yielded the same results (Fig 6F), suggesting that β-catenin is essential for the interaction between Plk1 and Ect2 during telophase. In addition, depletion of β-catenin reduced midbody localization of Ect2 during telophase as evidenced by an almost 50% reduction in Ect2 signal intensity at the midzone/midbody (Fig 6G and H). We measured the relative thickness of the neck (furrow ingression) in control and β-catenin-knockdown telophase cells (Appendix Fig S6A). Although slight furrow ingression was observed in β-catenin-depleted cells, the necks of β-catenin-knockdown cells were significantly thicker than those of control-knockdown cells. shControl cells represented less than 40% of the relative thickness of the neck, but shβ-catenin cells represented more than 60% of that. This phenomenon may be explained by a small amount of residual Ect2 localization due to incomplete knockdown of endogenous β-catenin in shβ-catenin cells. From these data, we speculated that the mislocalization of Ect2 by β-catenin depletion causes incomplete furrow ingression (Appendix Fig S6A). However, the stage of furrow ingression (such as initiation, progression, or completion) that can be regulated by the β-catenin–Ect2 axis should be defined in a further study.

We next investigated whether β-catenin also affects RhoA activity by comparing activity between WT and β-catenin-knockdown cells. RhoA exists as an inactive GDP-bound form and an active GTP-bound form, and active (GTP-bound) RhoA preferentially binds to the downstream effector rhotekin via a Rho-binding domain (RBD). Therefore, we assessed RhoA activity changes in control GL and β-catenin-knockdown cells by pull-down assays using GST–Rhotekin-RBD beads. Consistent with modulation of RhoA activation by β-catenin, RhoA pull-down by GST–Rhotekin-RBD beads was significantly reduced in β-catenin-knockdown cells; however, β-catenin had no effect on total RhoA protein levels, indicating that this effect was not mediated by changes in expression (Fig 6I and Appendix Fig S6B).

Immunoblotting was then performed to assess whether β-catenin depletion also affects the protein levels of various cytokinetic factors

© 2021 The Authors

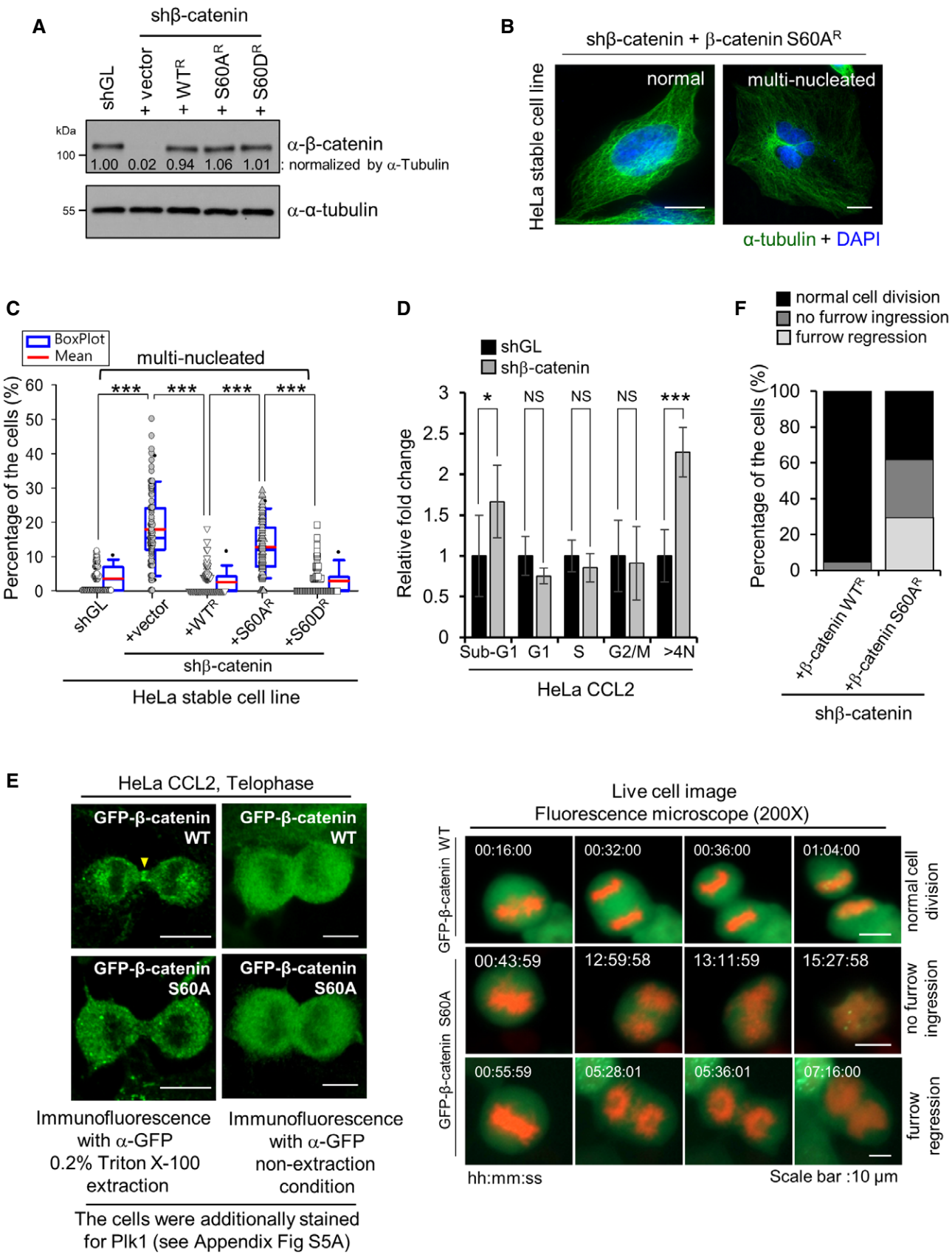

Figure 5.

© 2021 The Authors

Figure 5. Requirement of β-catenin Ser60 phosphorylation for cytokinesis.

A–C HeLa CCL2 cells stably expressing control vector only (+vector), β-catenin WT (+WT^R), S60A mutant (+S60A^R), or S60D mutant (+S60D^R) were generated using lentiviral infection and then infected with β-catenin-knockdown lentivirus (shβ-catenin). To confirm successful depletion of endogenous β-catenin and the expression of exogenous genes, the resulting cells were immunoblotted with the indicated antibodies (A). Band intensities were quantified using the ImageJ program and normalized with α-Tubulin, and the relative values of band intensities are marked. Cytokinesis-defective cellular phenotypes of each stable cell line were observed under a microscope using immunostained samples (B) and counted (C). A dot density graph with a box plot shows the percentage (%) of cells with cytokinesis-defective phenotypes (C). The box plot represents: central blue band, median; box, interquartile range; upper whisker, maximum observation below upper fence; lower whisker, minimum observation above lower fence; dot, outlier. Each symbol in the graph represents a percentage of more than 30 cells from three independent experiments. ***$P < 0.001$ (one-way ANOVA); scale bars, 10 μm.

D HeLa CCL2 cells infected with either control luciferase (shGL) or β-catenin (shβ-catenin) knockdown virus were subjected to FACS analysis. ***$P < 0.001$; *$P < 0.05$; NS, not statistically significant (unpaired two-tailed *t*-test). Error bars, S.D. from three independent experiments.

E, F HeLa CCL2 cells transiently transfected with either GFP–β-catenin WT or GFP–β-catenin S60A were monitored during cell cycle progression by live-cell imaging (E). The subcellular localizations of GFP-tagged β-catenin WT or S60A mutant construct were confirmed by immunofluorescence with anti-GFP antibody. The cells were additionally stained for Plk1 (see Appendix Fig S5A). The specific localization of GFP-β-catenin WT at the midbody was observed under a confocal laser microscope with high magnification (E, left panel). Cytokinesis-defective cellular phenotypes in each transfected HeLa cell were monitored (E, right panel) and counted using video clips (F). mCherry–Histone H2B was co-transfected with each GFP–β-catenin construct to visualize chromosomes. All live-cell images and video clips show representative data of more than 50 telophase cells in each experimental group. Arrowhead indicates GFP−β-catenin WT located at the midbody in telophase HeLa CCL2 cells. Scale bars, 10 μm.

Source data are available online for this figure.

including Ect2. Depletion of β-catenin did not affect protein levels of cytokinetic factors, including Ect2, suggesting that β-catenin specifically influences midbody recruitment of Ect2 (Appendix Fig S7A). In addition, expression of a constitutively active β-catenin mutant, β-catenin S45A, that accumulates in the nucleus to form complexes with Tcf/Lef and increase the transcriptional activity of target genes, also had no effect on the protein levels of cytokinetic factors, suggesting that β-catenin does not influence midbody localization of cytokinetic factors through effects on expression (Appendix Fig S7B). Alternatively, Wnt signaling is known to play an important role in cell proliferation; hence, whether the canonical Wnt/β-catenin pathway affects cytokinetic factor expression was investigated by immunoblot analysis following stimulation of cells with a control or a Wnt3a-conditioned medium (CM). Stimulation by Wnt3a increased β-catenin stabilization; however, it did not show significant changes in the levels of Ect2 and RhoA in telophase cells (Appendix Fig S7C). In addition, inhibition of Wnt signaling by IWP (an inhibitor of Wnt processing and secretion) treatment did not cause significant changes in the levels of Ect2 and RhoA in telophase cells (Appendix Fig S7D).

The TopFlash/FopFlash luciferase assay was performed to determine whether the Wnt/β-catenin pathway is activated during mitosis. In the absence of Wnt stimulation, low basal TopFlash levels were observed in both asynchronously growing cells and mitotic cells when compared to FopFlash levels, which was used as a negative control. However, Wnt activation by Wnt3a CM treatment in mitotic cells showed significantly higher TopFlash levels than that in asynchronously growing cells (Appendix Fig S7E). Thus, although Wnt signaling did not induce significant changes in the levels of Ect2 and RhoA in telophase cells, mitotic cells were more responsive to Wnt than asynchronously growing cells.

In addition, activation of Wnt signaling by Wnt3a CM treatment did not produce significant changes in Ect2−β-catenin complex formation in telophase cells (Appendix Fig S8A). Ect2 bound to a similar amount of β-catenin in both conditions compared to the control. RhoA activation was also unaffected by activation of Wnt signaling in telophase cells (Appendix Fig S8B). These results suggest that depletion of β-catenin influences the interaction between Ect2 and Plk1 and that their midbody localization occurs through transcription-independent mechanisms.

Plk1 activity-dependent phosphorylation of β-catenin Ser60 is essential for formation of the β-catenin–Plk1−Ect2 complex and activation of RhoA

We next investigated whether Plk1 activity affects the interaction between β-catenin and Ect2. Cells were treated with a high concentration (1 μM) of the Plk1 inhibitor BI 2536 for 20 min and protein localization was monitored by immunohistochemistry. To ensure that BI 2536 had successfully inhibited Plk1, immunocytochemistry was first performed using anti-Plk1 pT210 antibodies to specifically measure activated Plk1. While total Plk1 was still localized at the midbody following BI 2536 treatment, midbody localization of phosphorylated T210 Plk1 was diminished, indicating that BI 2536 had successfully inhibited Plk1 activity at the midbody (Appendix Fig S9A–D). Immunocytochemistry also revealed that BI 2536 abolished the localization of Ect2 at the midbody during telophase (Fig 7A and B). Thus, Plk1 activity is necessary for localization of Ect2 at the midbody during telophase. Surprisingly, treatment with BI 2536 did not affect the localization of endogenous total β-catenin but did reduce β-catenin p-S60 localization at the midbody as evidenced by quantification of immunofluorescence signals (Fig 7A and B; Appendix Fig S9E and F). Interestingly, BI 2536 treatment did not change the midbody localization of the exogenous GFP−β-catenin WT in telophase cells (Appendix Fig S9G). These findings were further confirmed by a midbody isolation assay. Midbodies isolated from telophase cells revealed that the inhibition of Plk1 by inhibitor treatment reduced the amount of β-catenin p-S60 compared to DMSO control. However, almost similar amounts of total β-catenin were observed between the control and Plk1 inhibitor-treated midbodies (Appendix Fig S9H and I). Collectively, these findings suggest that Plk1 activity is essential for β-catenin Ser60 phosphorylation at the midbody, which then may induce Ect2 recruitment. In addition, we measured the fluorescence signal intensities of Ect2 and Plk1 at the midbody in cell lines expressing WT, S60A, or S60D β-catenin. We found that the signal intensity of Plk1 at the midbody was not significantly different between the three cell lines but that of Ect2 was significantly diminished in the cell line expressing S60A β-catenin compared to those expressing WT or S60D β-catenin (Appendix Fig S10A and B). This reflects the possibility that Ect2 recruitment after β-catenin Ser60 phosphorylation.

© 2021 The Authors

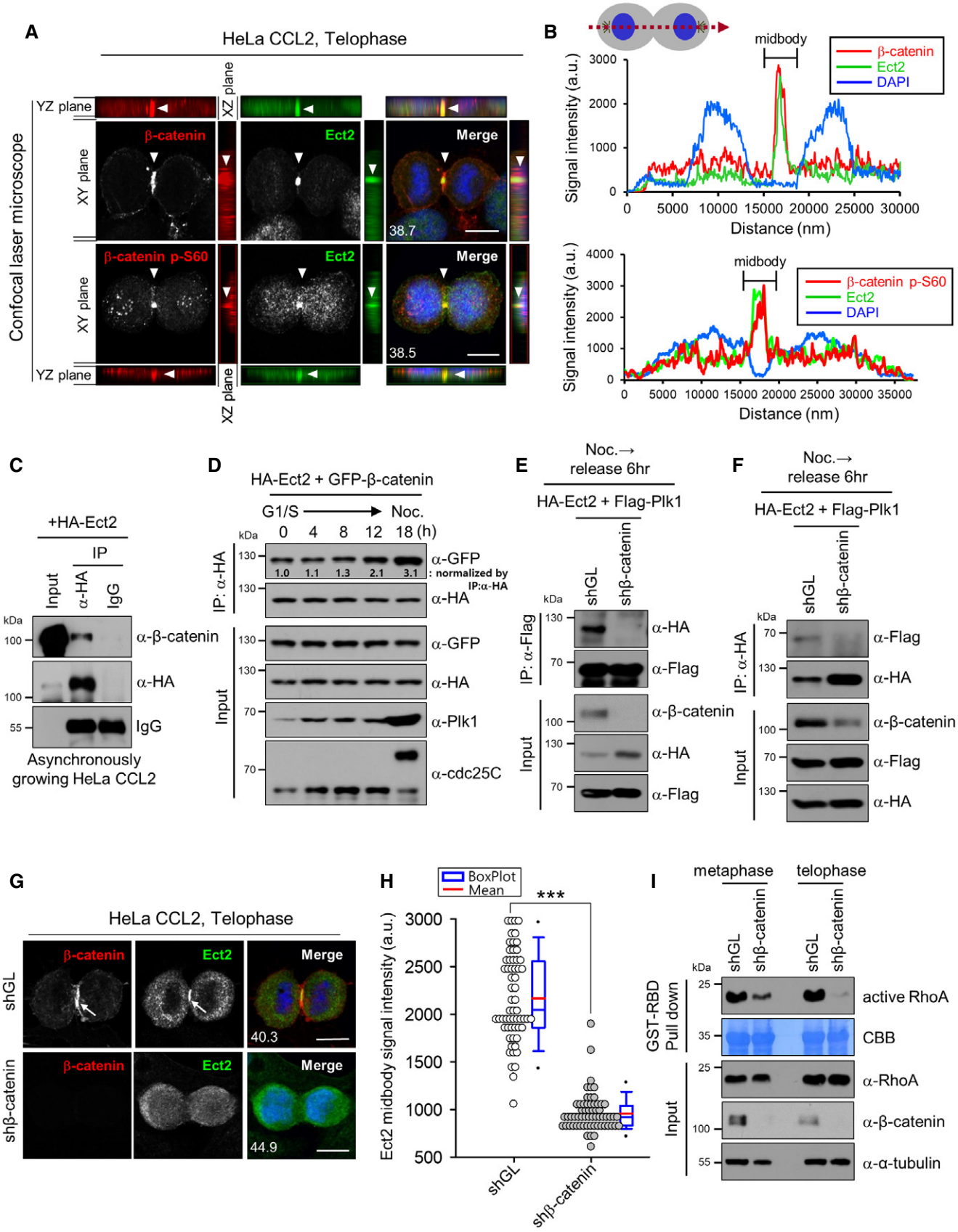

Figure 6.

© 2021 The Authors

Figure 6. β-Catenin mediates Ect2–Plk1 interaction, RhoA activation, and midbody localization of Ect2.

A Asynchronously growing HeLa CCL2 cells were immunostained with the indicated antibodies after extraction using 0.2% Triton X-100. The resulting samples were observed using a confocal laser microscope (Zeiss LSM 700). Scale bars, 10 μm. The value of the relative neck thickness is shown in the lower left corner of the merged images (A). Arrowheads indicate Ect2, total β-catenin, and β-catenin p-S60 located at the midbody in telophase HeLa CCL2 cells.

B Intercentrosomal (centrosome-to-centrosome) linear signal profiles of β-catenin/Ect2 (upper panel) and β-catenin p-S60/Ect2 (lower panel) from the XY plane of the immunostained cells in (A). All immunofluorescence images and linear signal profiles show representative data of more than 50 telophase cells obtained from three independent experiments (A, B).

C Asynchronously growing HeLa CCL2 cells were transfected with HA–Ect2. The resulting cells were used for immunoprecipitation analysis using either anti-HA antibody or non-immunized mouse IgG control. Precipitates were separated by 10% SDS–PAGE and immunoblotted with the indicated antibodies.

D HeLa CCL2 cells co-transfected with HA–Ect2 and GFP–β-catenin were synchronized using a double thymidine block and released using medium containing 200 ng/ml nocodazole (Noc.) at the indicated time point. Cells at each release time point were harvested and used for immunoblot analysis using anti-HA antibodies. Immunoprecipitated beads were analyzed by SDS–PAGE followed by immunoblot analysis. Band intensities were quantified using the ImageJ program and normalized to the level of immunoprecipitated HA-Ect2 protein, and the relative values of band intensities are marked.

E, F HeLa CCL2 cells infected with the indicated lentiviruses were co-transfected with HA–Ect2 and Flag–Plk1. Cells were then treated with nocodazole (200 ng/ml) for 18 h and released from cell cycle arrest by incubation in fresh medium for 6 h. The resulting cells were used for immunoprecipitation analysis using anti-Flag (E) or anti-HA (F) antibodies. Precipitated beads were used for immunoblot analysis using the indicated antibodies.

G, H HeLa CCl2 cells infected with either sh-control luciferase (shGL) or shβ-catenin lentiviruses were co-immunostained with anti-β-catenin and anti-Ect2 antibodies. Localization of β-catenin and Ect2 in the midbody of telophase cells was observed using a confocal microscope (G) and the signal intensity of Ect2 was monitored in the midbody of each knockdown telophase cell (H). Arrows indicate total β-catenin and Ect2 located at the midbody in telophase HeLa CCL2 cells (G). A dot density graph with a box plot shows the signal intensity of midbody-localized Ect2 in telophase cells. The box plot represents: central blue band, median; box, interquartile range; upper whisker, maximum observation below upper fence; lower whisker, minimum observation above lower fence; dot, outlier. Approximately 70 cells from three independent experiments were measured. ***$P < 0.001$ (unpaired two-tailed t-test); Scale bars, 10 μm. The value of the relative neck thickness is shown in the lower left corner of the merged images (G).

I HeLa CCL2 cells infected with either sh-control luciferase (shGL) or shβ-catenin lentiviruses were treated with nocodazole (200 ng/ml) for 18 h (metaphase) and released by incubation in fresh medium for 2 h (telophase). Cell lysates were analyzed by pull-down assays using rhotekin-RBD beads, and pulled down proteins were separated by SDS–PAGE followed by immunoblot analysis using the indicated antibodies. The membrane was then stained with Coomassie (CBB) to confirm the amount of RBD precipitated.

Source data are available online for this figure.

The failure of β-catenin p-Ser60 and Ect2 to localize at the midbody following Plk1 inhibitor treatment further suggests that Plk1 activity facilitates the interaction between β-catenin and Ect2. To confirm this hypothesis, late mitosis/telophase cell lysates from HeLa CCL2 cells transfected with HA–Ect2 and treated with vehicle (DMSO) or BI 2536 for the indicated times were examined by immunoprecipitation. Consistent with modulation of the β-catenin−Ect2 interaction by Plk1-mediated phosphorylation, co-immunoprecipitation of β-catenin and Ect2 was reduced in a time-dependent manner by BI 2536 treatment compared to vehicle (Fig 7C). The requirement of Plk1 for Ect2−β-catenin binding was further confirmed by Plk1 knockdown. Depletion of Plk1 severely impaired the interaction between HA-Ect2 and endogenous β-catenin compared with control knockdown (Fig 7D). Alternatively, expression of a HA-labeled constitutively active Plk1, HA-Plk1 T210D significantly increased the interaction between endogenous Ect2 and GFP-β-catenin compared to vector control or the inactive HA-Plk1 K82M mutant (Fig 7E).

Additionally, immunoprecipitation revealed that substitution of Ser60 with Ala60 dramatically reduced the interaction with Ect2 compared to WT β-catenin, while Ect2 binding to the S60D β-catenin mutant was significantly higher than to WT β-catenin (Fig 7F). Next, we sought to clarify the direct or indirect nature of the interaction between β-catenin and Ect2 by performing a GST pull-down assay using bacterially purified GST-β-catenin (WT, S60A, or S60D) and His/GST-Ect2. Under the conditions of direct interaction between bacterially purified GST-Ect2 and His-Ect2 (homodimerization), neither GST-β-catenin WT, S60A, nor S60D interacted with His-Ect2 in the GST pull-down assay (Appendix Fig S11). Therefore, we concluded that the interaction between β-catenin and Ect2 in immunoprecipitation is indirect. With these results, we presume that in the interaction between β-catenin and Ect2, β-catenin phosphorylation could bring about a number of changes that allow for interactions between these proteins that need not be direct binding of a phospho-epitope.

The importance of β-catenin Ser60 phosphorylation by Plk1 for RhoA activity was also confirmed, as GTP–RhoA levels revealed by rhotekin-RBD pull-down were reduced by expression of the β-catenin S60A mutant compared to the WT or S60D β-catenin mutant in both metaphase and telophase cells (Fig 7G). Thus, phosphorylation of β-catenin Ser60 by Plk1 activity promotes the interaction with Ect2 and thereby increases RhoA activity at the midbody during telophase.

Discussion

The present study identifies a novel Plk1 phosphorylation site on β-catenin (Ser60) that localizes at the midbody (β-catenin p-S60 is surrounded by actomyosin contractile ring) during early telophase. The phosphorylation of β-catenin Ser60 allows interaction with the Rho-GEF Ect2 and thereby recruits Ect2 to the midbody, where it activates RhoA. We further demonstrate that this continuous pathway is essential for the completion of cytokinesis (Fig 8).

More than 20 β-catenin phosphorylation residues have been identified and characterized, but the p-S60 epitope is functionally distinct. Typically, β-catenin phosphorylation occurs first at Ser45 by CK1α, followed by phosphorylation at Ser33, Ser37, and Thr41 by GSK3β. This multiphosphorylated β-catenin is recognized by a specific E3 ubiquitin ligase ($SCF^{\beta\text{-}TrCP}$) and eventually degraded by the 26S proteasome (Liu *et al*, 1999, 2002; Winston *et al*, 1999; Wu & He, 2006). This degradation machinery of β-catenin is an important regulator of the canonical Wnt signaling pathway. In contrast, the β-catenin p-S60 epitope discovered in this study is functionally

© 2021 The Authors

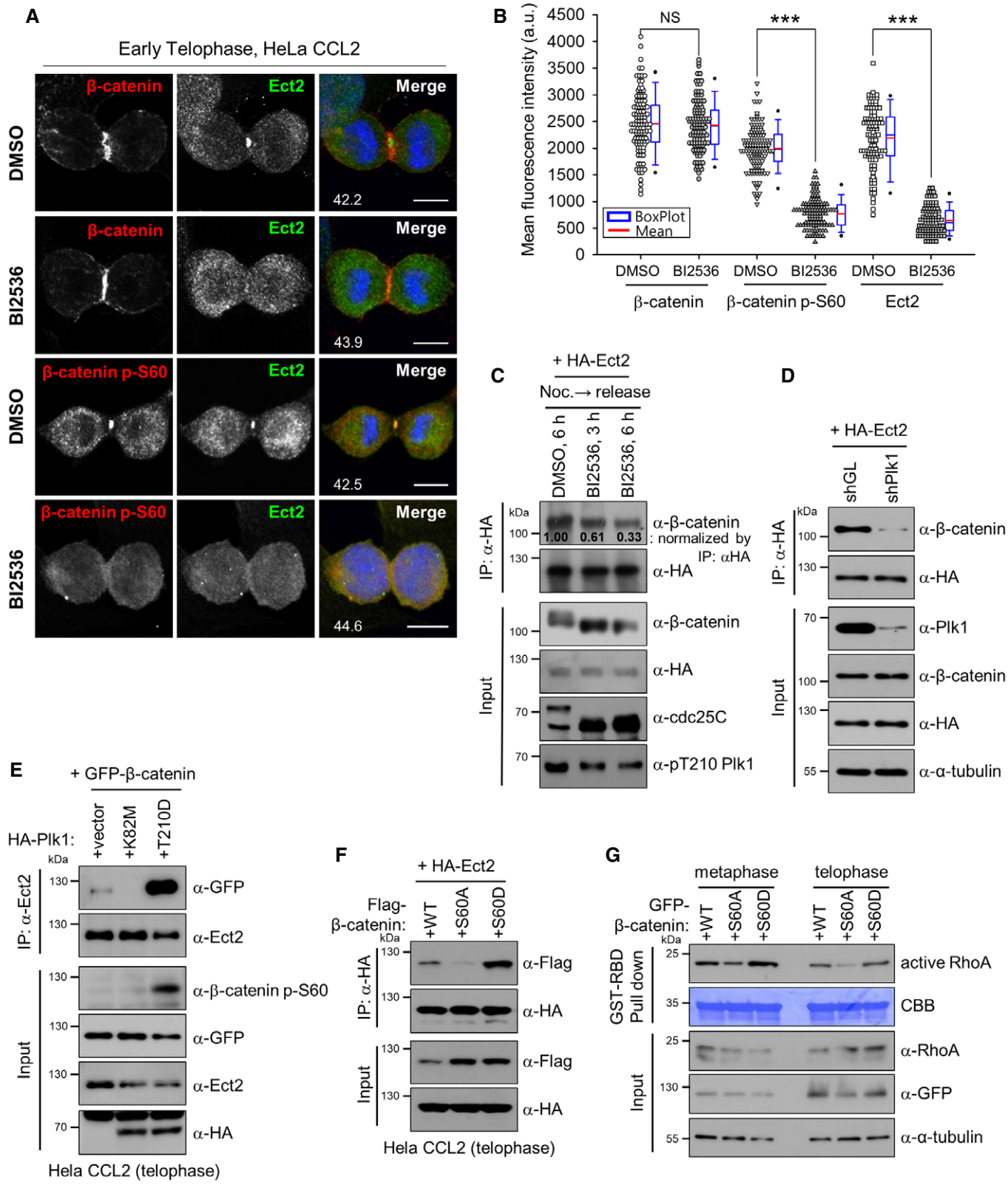

Figure 7.

© 2021 The Authors

Figure 7. Phosphorylation of β-catenin Ser60 by Plk1 activity is essential for midbody localization of Ect2, activation of RhoA, and the interaction between β-catenin and Ect2.

A, B HeLa CCL2 cells treated with DMSO (control) or the Plk1 inhibitor, BI 2536 (1 μM) for 20 min were immunostained with a combination of either anti-total β-catenin and anti-Ect2 antibodies or anti-β-catenin p-S60 and anti-Ect2 antibodies (A). Scale bars, 10 μm. The signal intensities of total β-catenin, β-catenin p-S60, and Ect2 were measured in the midbody of compound-treated telophase cells (B). A dot density graph with a box plot shows the signal intensity of midbody-localized β-catenin, β-catenin p-S60, or Ect2 in telophase cells. The box plot represents: central blue band, median; box, interquartile range; upper whisker, maximum observation below upper fence; lower whisker, minimum observation above lower fence; dot, outlier. More than 100 cells from three independent experiments were measured. ***$P < 0.001$; NS, not statistically significant (unpaired two-tailed *t*-test); Scale bars, 10 μm. The value of the relative neck thickness is shown in the lower left corner of the merged images (A).

C After 18 h of nocodazole (200 ng/ml)-induced cell cycle arrest, HeLa CCL2 cells transfected with HA–Ect2 were released by incubation in fresh medium for 2 h and treated with either DMSO (control) or Plk1 inhibitor (BI 2536) for the indicated times. The resulting cells were used for immunoprecipitation analysis using anti-HA antibody, and immunoprecipitates were separated by SDS–PAGE followed by immunoblot analysis with the indicated antibodies. The band intensity of β-catenin bound to HA-Ect2 was quantified with ImageJ and normalized to the signal intensity of immunoprecipitated HA-Ect2, and the relative values are shown below the bands.

D HeLa CCL2 cells transfected with HA–Ect2 were infected with sh-control luciferase (shGL) or shPlk1 lentiviruses. The resulting cells were used for immunoprecipitation analysis using anti-HA antibody, and immunoprecipitates were separated by 10% SDS–PAGE followed by immunoblot analysis with the indicated antibodies.

E HeLa CCL2 cells were co-transfected with GFP−β-catenin (+GFP–β-catenin) and either empty vector (+vector, control), HA–Plk1 kinase-dead mutant (+KM), or HA–Plk1 constitutively active mutant (+T210D), then treated with 200 ng/ml nocodazole for 18 h and released by incubation in fresh medium for 2 h (telophase). The resulting cells were used for immunoprecipitation analysis with anti-Ect2 antibodies. Immunoprecipitated beads were separated by 10% SDS–PAGE followed by immunoblot analysis using the indicated antibodies.

F HeLa CCL2 cells were co-transfected with HA–Ect2 and either wild-type Flag–β-catenin (+WT), Flag–β-catenin S60A mutant (+S60A), or Flag–β-catenin S60D mutant (+S60D) and then treated with 200 ng/ml nocodazole for 18 h and released by incubation in fresh medium for 2 h (telophase). The resulting cell lysates were used for immunoprecipitation analysis with anti-HA antibody. Immunoprecipitated beads were separated by 10% SDS–PAGE followed by immunoblot analysis with the indicated antibodies.

G HeLa CCL2 cells were transfected with either wild-type Flag−β-catenin (+WT), Flag–β-catenin S60A mutant (+S60A), or Flag–β-catenin S60D mutant (+S60D), then treated with 200 ng/ml nocodazole for 18 h (metaphase) and released by incubation in fresh medium for 2 h (telophase). Cell lysates were used for pull-down analysis with rhotekin–RBD beads, and the pulled down beads were separated by 12% SDS–PAGE followed by immunoblot analysis with the indicated antibodies. The membrane was then stained with Coomassie (CBB) to determine the amount of RBD precipitated.

Source data are available online for this figure.

distinct from other known phosphorylation sites. First, unlike other Plk1 substrates, the physical interaction with β-catenin prior to phosphorylation did not require a priming phosphorylation event. In addition, the low level of basal TopFlash during mitosis was found (Appendix Fig S7E), and activation or inhibition of canonical Wnt signaling did not induce significant changes in the levels of cytokinetic factors Ect2, Anillin, RhoA, and Mklp2 in telophase cells (Appendix Fig S7C and D). High levels of endogenous β-catenin in the mitotic phase were reported (Davidson *et al*, 2009; Fig 1B), but in the absence of Wnt stimulation, low basal TopFlash levels have been observed in asynchronously growing and mitotic cells compared to FopFlash levels (Appendix Fig S7E). Wnt3a stimulation induced significantly higher levels of TopFlash compared to FopFlash in both asynchronously growing and mitotic cell conditions. Consistent with the previous report (Davidson *et al*, 2009), Wnt stimulation generated higher TopFlash levels in mitotic cells than in asynchronously growing cells. However, in the absence of Wnt stimulation, the level of TopFlash in mitotic cells increased slightly compared to that in asynchronously growing cells. Moreover, there were no significant differences between the values of TopFlash and FopFlash (basal level). It is difficult to deduce whether a slight increase in TopFlash level is significant in mitotic cells compared to asynchronously growing cells because a previous report (Davidson *et al*, 2009) did not show the level of FopFlash in the absence of Wnt stimulation. However, considering our results and the previous report, it is assumed that mitotic cells contain more Wnt responsiveness than asynchronously growing cells.

Thus, phosphorylation of Ser60 by Plk1 indicated by a SDS−PAGE mobility shift (Fig 1A–D) was critical for cytokinesis but appeared independent of canonical Wnt signaling. However, the function of β-catenin p-S60 in canonical Wnt signaling requires further investigation. Interestingly, the β-catenin Ser60 residue was conserved within, but not beyond, mammals (Fig 2E). It is possible that evolutionarily, the role of β-catenin Ser60 phosphorylation (p-S60) in cytokinesis may have emerged relatively recently. Therefore, the function of p-S60 in cytokinesis is confined to mammalian species, and other β-catenin phosphorylation sites may perform this function beyond the class Mammalia. Although in the present study, we focused on the important function of phosphorylation of an N-terminal β-catenin residue (Ser60), phosphorylation in the C-terminal portion of β-catenin is also reported to be important for various cellular processes. Previous studies have indicated that phosphorylation of β-catenin at Ser552 and Tyr654 is important for its transcriptional activity and binding to E-cadherin, respectively (Roura *et al*, 1999; Fang *et al*, 2007). Thus, C-terminal phosphorylation of β-catenin is also dispensable for the cellular function of β-catenin.

The Rho-GEF Ect2 is a known cytokinesis regulator and Ect2−RhoA network is regulated by Plk1 activity during the initiation of cytokinesis (Burkard *et al*, 2007; Petronczki *et al*, 2007; Santamaria *et al*, 2007). It has also been reported that the phosphorylation of the Ect2 Thr412 residue by Cdk1 is essential for Plk1-PBD binding and cell division (Niiya *et al*, 2006). In this study, we demonstrate that β-catenin Ser60 phosphorylation by Plk1 is necessary for midbody localization of Ect2 (Figs 6G and H, and 7A and B). In the absence of β-catenin p-S60, Ect2 was not recruited to the midbody and RhoA activity was also decreased (Fig 7A–G). These results strongly suggest that β-catenin p-S60 may act upstream of RhoA, but further studies are needed to confirm this notion.

© 2021 The Authors

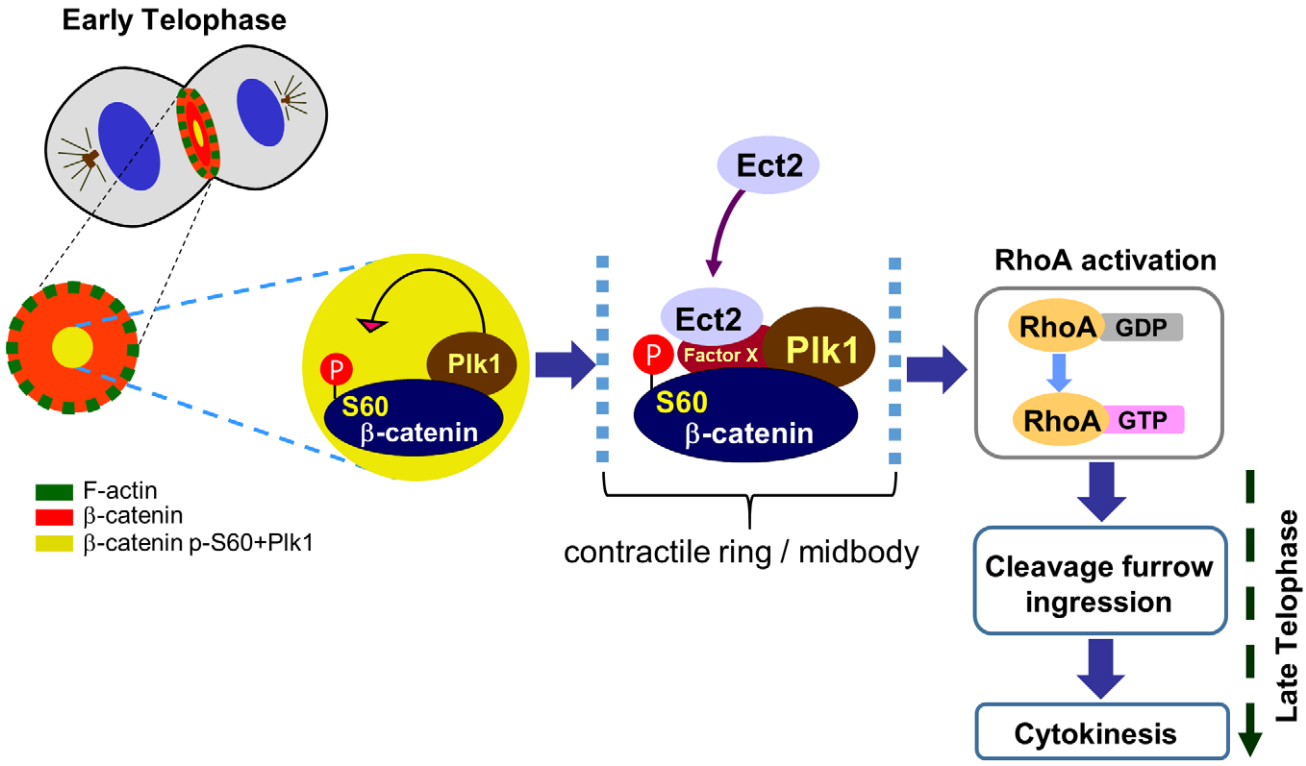

Figure 8. Proposed function of β-catenin in cytokinesis.

During mitotic progression, β-catenin binds to Plk1 PBD in a phosphorylation-independent manner and localizes at the midbody/contractile ring of telophase cells (β-catenin p-S60 is surrounded by actomyosin contractile ring during early telophase). The Ser60 residue of β-catenin is phosphorylated by bound Plk1, which recruits Ect2 to the midbody and facilitates the formation of the β-catenin–Plk1–Ect2 complex. The resulting complex induces RhoA activation and mediates the progression of cleavage furrow ingression and subsequent cytokinesis steps.

Almost all known Plk1 substrates exhibit phosphorylation-dependent binding to Plk1-PBD. This means that Plk1 phosphorylation is dependent on prior phosphorylation by other kinases (called priming kinases) at distinct sites. Surprisingly, however, β-catenin bound to Plk1-PBD in a phosphorylation-independent manner (Fig 1E–G). This combination of phosphorylation-independent and phosphorylation-dependent binding enhances the functional diversity of Plk1 substrates.

The slower-migrating β-catenin protein band on SDS–PAGE representing Plk1-phosphorylated β-catenin was also observed in the early mitotic phase (G2/M) (Fig 1). This implies the possibility that β-catenin p-S60 can function in metaphase (early mitosis) as well as in telophase (late mitosis). Plk1 is a key regulator of mitotic progression, and recently, its non-mitotic functions have also been identified (Barr *et al*, 2004; Petronczki *et al*, 2008; Kishi *et al*, 2009; Lee *et al*, 2012, 2017, 2018). Therefore, the well-studied Plk1 functions in early mitosis (metaphase) also support the potential dual/multiple functions of β-catenin p-S60 during cell cycle progression. In this study, the cytokinetic functions of β-catenin p-S60 were revealed by immunostaining, which showed Plk1 activity-dependent localization at the midbody and failure of cytokinesis upon disruption of Plk1-mediated S60 phosphorylation. However, it is also possible that β-catenin p-S60 functions in concert with Plk1 during early mitotic events such as mitotic entry, centrosome maturation, or kinetochore attachment.

Cytokinesis is a highly dynamic process involving multiple networks of various factors. In this study, a new function of β-catenin in cytokinesis was elucidated that depends on Plk1-mediated phosphorylation, and the formation of a β-catenin p-S60–Plk1–Ect2 complex at the midbody was found. In addition, based on their localization in early telophase cells, β-catenin is presumed to be one of the contractile ring components, and the phosphorylation of β-catenin S60 by Plk1 is likely to induce contractility. Identification of additional factors that interact functionally with this complex is critical for a better mechanistic understanding of cytokinesis.

Cytokinesis failure is one cause of genomic instability and tumorigenesis (reviewed extensively elsewhere; Eggert *et al*, 2006; Lens & Medema, 2019). Therefore, a fully comprehend the complicated nature of cytokinesis is crucial to overcome cancers. The mechanistic insights provided by this study may provide fundamental knowledge for future cancer research.

Materials and Methods

Plasmid construction and mutagenesis

*Bam*HI-*Not*I fragments of mouse *β-catenin* wild-type (WT) or various mutants [each a truncation (T1, T2, and T3 mutants) and an

 © 2021 The Authors

alanine ("A") / aspartic acid ("D") substitution mutant] were amplified by polymerase chain reaction (PCR) from the *pCDNA3-Flag-β-catenin* WT (a gift from Eric R. Fearon, University of Michigan, MI) and the *pEGFP-C1-β-catenin WT* (a gift from W. James Nelson, Stanford University, CA). The PCR products were digested with the corresponding restriction enzymes and sub-cloned into *pcDNA-FLAG* (Invitrogen, Carlsbad, CA) and *pGEX-4T-2* (Amersham Biosciences, Piscataway, NJ) vectors. *Sal*I fragments were generated for sub-cloning into *pHR′-CMV-SV-puro* (a gift from Kyung S. Lee, NIH/NCI, Bethesda, MD) vectors. PCR-based site-directed mutagenesis was used to generate mutant constructs.

*Eco*RI-*No*tI or *Bam*HI-*Xho*I fragments of Ect2 were amplified by PCR from the *pFUGW-HA ECT2* (a gift from Adrienne D. Cox, University of North Carolina, NC), and the PCR products were sub-cloned into *pGEX-4T-2* or *pET-28b*(+) (Novagen) vectors, respectively.

To generate lentivirus-based *β-catenin* shRNA (sh1746)-expressing constructs, the oligonucleotide sequences from the human *β-catenin* (accession no. BC058926) open reading frame (nt 1746 ~ 1769; forward 5′-CCGGGGATGTTCACAACCGAATTGTTATGCTAGC ATAACAATTCGGTTGTGAACATCCTTTTTG-3′ and reverse 5′-AATTCAAAAAGGATGTTCACAACCGAATTGTTATGCTAGCATAACAATTCGGTTGTGAACATCC-3′; the targeting sequences are underlined) were annealed and sub-cloned into the *Age*I-*Eco*RI site of the *pLKO.1-puro* vector (a gift from Sheila A. Stewart and Phillip A. Sharp, MIT, Cambridge, MA).

The mouse *β-catenin* constructs bearing silent mutants against the human *β-catenin* sh1746 RNA sequence contain three different nucleotides from human *β-catenin* sequences (5′- ggacgttcacaaccggattgtaat −3′; three different nucleotides are underlined). The target sequences of shGL {CGTACGCGGAATACTTCGA (Elbashir *et al*, 2001)} and shPlk1 {AGATTGTGCCTAAGTCTCT (Lee *et al*, 2012)} was sub-cloned into *pLKO.1-puro* vector in the same manner to produce *β-catenin* shRNA (sh1746).

Cell culture, transfection, synchronization, and inhibitor treatment

HeLa CCL2, HEK293T, NRK, MRC-5, 267B1, and MEF cell lines were obtained from American Type Culture Collection (ATCC; Manassas, VA) and cultured as recommended by ATCC. Control or Wnt3a-conditioned medium (CM) were generated from control or *Wnt3a*-expressing stable mouse L-fibroblast cell lines (a gift from Sean B. Lee, Tulane University School of Medicine, New Orleans, LA), respectively. Plasmids were transfected to cells using X-tremeGENE HP DNA transfection reagent (Roche, Basel, Switzerland) or Lipofectamine 2000 (Invitrogen, Carlsbad, CA) according to the manufacturer's instructions.

To inhibit CK1δ/ϵ, CK1δ, Plk1, GSK3β, CDK2/5/1/9, Aurora kinase A/B, or Aurora kinase A, HeLa CCL2 cells were treated with 40 μM of IC261 (Selleckchem, Houston, TX), 20 μM of D4476 (Sigma-Aldrich, St. Louis, MO), 100 nM of BI2536 (Selleckchem), 5 μM of TWS119 (Selleckchem), 25 nM of Dinaciclib (Selleckchem), 2 μM of ZM447439 (Selleckchem), or 500 nM of VX680 (Selleckchem) for 1 h, respectively. To inhibit Wnt signaling, HeLa CCL2 cells were treated with 10 μM of IWP-2 (Sigma-Aldrich) for 18 h.

For the double thymidine block and release experiment, HeLa CCL2 cells were arrested for 18 h with 2.5 mM thymidine (Sigma, St. Louis, MO) and then released with fresh medium for 9 h. The arrest-release cycle was repeated twice. After the second arrest cycle, cells were released either with fresh medium for 18 h to follow cell cycle progression or with 200 ng/ml of nocodazole (Sigma) contained medium for 18 h to arrest the cells at prometaphase.

Lentivirus generation and stable cell line generation

For the generation of the shRNA lentiviruses, *pLKO.1-puro-shLuciferase* (shGL) or *pLKO.1-puro-shβ-catenin* (shβ-catenin) construct was co-transfected with *pHR'-CMV-VSV-G* (protein G of vesicular stomatitis virus) and *pHR′-CMVΔR8.2Δvpr* into HEK293T cells. To generate protein expressing lentiviruses, *pHR′- CMV-SV-puro-vector* only, *pHR′- CMV-SV-puro-β-catenin wild-type*^{R} (R, sh1746-resistant mouse *β-catenin*), *S60A*^{R}, or *S60D*^{R} construct was co-transfected with *pHR'-CMV-VSV-G* and *pHR′-CMVΔR8.2Δvpr* into HEK293T cells.

To generate expression-knockdown stable cell lines expressing wild-type β-catenin and various β-catenin mutants, HeLa CCL2 cells were first infected with the expression lentiviruses for 1 day and then selected with 4 μg/ml of puromycin for 2–3 days. The expression stable cell lines were then infected with the high titer of knockdown lentiviruses.

Immunoprecipitation and immunoblot analysis

Immunoprecipitation was carried out as described previously (Lee *et al*, 2018). Briefly, cells harvested with 1× ice-cold phosphate-buffered saline (PBS) were lysed in 1× TBSN buffer {20 mM Tris–Cl (pH 8.0), 0.5% NP-40, 150 mM NaCl, 5 mM EGTA, 1.5 mM EDTA, 0.5 mM Na_3VO_4, 10 mg/ml pNPP (p-nitrophenyl phosphate; Sigma), and a protease-inhibitor cocktail (Roche, Mannheim, Germany)}. The resulting total cell lysates were then centrifuged at 15,000× *g* for 20 min at 4°C. Each antibody was added to clear lysates (1–1.5 mg) and incubated for 4–6 h at 4°C. Protein A or G–sepharose beads (Santa Cruz Biotechnologies, Santa Cruz, CA) were then added to antibody containing cell lysates and incubated for additional 2 h at 4°C. Resulting immunoprecipitated proteins were separated by 8–12% sodium dodecyl sulfate-polyacrylamide gel electrophoresis (SDS–PAGE) and transferred to PVDF membrane. Samples were separated by 10% low-bis acrylamide gel to reveal hyperphosphorylated β-catenin proteins.

PVDF membranes were sequentially incubated with primary antibodies for 2–4 h at room temperature (or overnight at 4°C) and horseradish peroxidase (HRP)-conjugated secondary antibodies (Cell Signaling, Danver, MA) for 1 h at room temperature. After extensive washing with 1×TBST [(50 mM Tris–Cl (pH 7.5), 0.05% Tween 20, 150 mM NaCl)], membranes were sprayed with enhanced chemi-luminescence (ECL) solution (Pierce, Rockford, IL) to detect immunoreactive signals. Lists and titrations of antibodies used in immunoblotting are shown in Appendix Table S1.

GST-PBD-binding assay and GST pull-down assay

To perform GST-PBD-binding assay, bead-conjugated GST-Plk1 PBD WT or GST-Plk1 PBD (10–20 μg) phosphopincer mutants (AM; H538A K540M) (a gift from Michael B. Yaffe, MIT, Cambridge, MA) was incubated with clear cell lysates (0.5–1 mg) prepared in 1×

© 2021 The Authors

TBSN buffer for 1 h at 4°C. The beads were then precipitated by brief centrifugation and washed 4 times with 1× TBSN buffer. The resulting samples were then subjected to immunoblot analyses as described above.

Bacterially purified GST-fusion proteins (GST, GST-β-catenin WT, S60A, S60D, or GST-Ect2) (3–6 μg) were mixed with bacterially purified His-Ect2 (3–6 μg) in 1× TBSN buffer for 1 h at 4°C. Glutathione (GSH)-agarose beads were added to each sample, and the bead-containing samples were incubated for an additional 1 h at 4°C. Bead-conjugated GST-Plk1 WT or GST was incubated with clear cell lysates (0.5–1 mg) prepared in 1× TBSN buffer for 1 h at 4°C. The beads were then precipitated by brief centrifugation and washed 4 times with 1× TBSN buffer. The resulting samples were then subjected to immunoblot analyses as described above.

Phospho-specific antibody production

The rabbit polyclonal anti-β-catenin pSer-60 antibody was generated by injection of synthetic phospho-peptides, NH_2-EDVDT-pS-QVLYE-COOH (55–65 amino acid) (AbFRONTIER Inc., Seoul, Korea). Immunized sera were monitored with enzyme-linked immunosorbent assay (ELISA) and immunoblot analysis. The final serum was purified by affinity chromatography. To increase specificity of anti-β-catenin pSer-60 antibody, 5 μg/ml of non-phosphopeptide (NH_2-EDVDT-S-QVLYE-COOH) was added to purified antibody.

In vitro kinase assay

To perform *in vitro* kinase assay, each of the *GST-β-catenin* WT, *GST-β-catenin* various alanine substitution mutants, and truncation mutants was expressed in *E. coli* BL21 (DE3) via isopropyl β-D-1-thiogalactopyranoside (IPTG) induction. The expressed proteins were then purified using glutathione (GSH)-agarose beads (Sigma). Both wild-type HA-Plk1 (WT) and kinase-inactive HA-Plk1 (K82M) (Lee *et al*, 1995) were purified from Sf9 cells. Flag-Plk1 was expressed in 293T cells transfected with Flag-Plk1 and was purified via immunoprecipitation with anti-Flag antibody. 3–5 μg of purified proteins was used per reaction. *In vitro* kinase assay was reacted in 1× kinase cocktail {5 mM dithiothreitol (DTT), 50 mM Tris–Cl (pH 7.5), 10 mM $MgCl_2$, 2 mM EGTA, 10 mg/ml pNPP (p-nitrophenyl phosphate; Sigma), and protease-inhibitor cocktail (Roche)} in the presence of 10 μM cold-ATP and 10 μCi [γ-^{32}P]ATP, for 30 min at 30°C. The resulting proteins were separated with SDS–PAGE, the gels were dried and exposed to X-ray film to get the autoradiogram.

Immunofluorescence assay, super-resolution confocal laser scanning microscope, and image analyses

Immunofluorescence analyses were performed essentially as described previously (Lee *et al*, 2017). To detect midbody localization of β-catenin WT, β-catenin p-S60, Plk1, and Ect2, the HeLa CCL2, NRK, MRC-5, 267B1, or MEF cells were fixed with 4% paraformaldehyde in DPBS for 10 min at room temperature. Cells were then washed with 1×PBS and permeabilized/fixed with −20°C cold methanol for 3 min. Subsequently, the resulting samples were extensively washed with 0.1% PBST (1× PBS + 0.1% Triton X-100) four times or more to remove the methanol remnant. Primary antibodies were incubated for 4 h at room temperature (or overnight at 4°C for phospho-specific antibody) and washed with 0.1% PBST three times or more. Texas Red-X /Alexa Fluor 488-conjugated secondary antibodies (Invitrogen) were incubated for 1 h at room temperature. 1 μg/ml of 4′,6′-diamidino-2-phenylindole (DAPI) (Sigma) solution was used to stain the DNA.

The resulting coverslips were mounted on the glass slides with a Fluoro-Gel mounting medium (EMS, Hatfield, PA). Fluorescent images were observed and photographed using either a Zeiss LSM 700 confocal microscope (Carl Zeiss, Oberkochen, Germany), Zeiss AxioObserver (Carl Zeiss), or Nikon Eclipse ti-u (Nikon, Tokyo, Japan) inverted fluorescence microscope system. Digital images (1,388 × 1,040 pixels and 12-bit resolution or 1,280 × 1,024 pixels and a 16-bit resolution) were analyzed by using the ImageJ (NIH) or the ZEN v2.1 (Carl Zeiss) software. To obtain super-resolution images, digital images were acquired and analyzed by using super-resolution confocal laser scanning microscope (LSM-880 with Airyscan, Carl Zeiss).

The transfected cells were subjected to immunostaining analysis with anti-GFP and anti-Plk1 antibodies. To confirm specific localizations of overexpressed *pEGFP-β-catenin WT*, *S60A*, or *S60D* construct, extraction step with 0.2% Triton X-100 buffer (100 mM PIPES pH 6.8, 5 mM EGTA, 1 mM $MgCl_2$, 0.2% Triton X-100) was proceeded before fixation. Resulting samples were subjected to immunostaining analysis with anti-GFP and anti-Plk1/anti-Plk1 p-T210 antibodies, as described above. Fluorescent-tagged β-catenin signals were observed and photographed using a Zeiss LSM 700 confocal microscope (Carl Zeiss).

Lists and titrations of antibodies used in immunofluorescence analyses are presented in Appendix Table S1.

Live-cell imaging analyses

HeLa CCL2 or HEK293T cells were grown on a μ-Dish 35 mm, high glass bottom (Ibidi GmbH, Martinsried, Germany), and then transfected with either *pEGFP-β-catenin WT* or *pEGFP-β-catenin S60A*. *pmCherry–Histone H2B* (a gift from Kunsoo Rhee, Seoul National University, Korea) was co-transfected with each *pEGFP–β-catenin* construct to visualize chromosomes. After 8 h of transfection, the culture dishes were mounted on an Axio Observer Z1 inverted fluorescence microscope (Carl Zeiss), equipped with a CO_2 and a temperature controller (Carl Zeiss), and the digital images were obtained under an A-Plan 20X/0.8 ph2M27 objective. Snapshots were acquired at every 4 min interval through the AxioCam MRm camera (Carl Zeiss), operated by the ZEN v2.1 (blue edition) software (Carl Zeiss), under 5% CO_2 and 37°C conditions. The generation of the live-cell movie and the analysis of the images were performed using the ZEN v2.1 (blue edition) software (Carl Zeiss).

Flow cytometry (FACS) analysis

The HeLa CCL2 cells treated with either control luciferase (shGL) or shβ-catenin lentiviruses for 1 day and then selected with 4 μg/ml of puromycin for 2 days. The resulting cells were then harvested by using trypsinization and reacted with BD cycletest™ Plus DNA reagent kit (BD Biosciences, CA) according to manufacturer's instructions. FACS analyses were performed by using BD FACSCalibur™ Flow Cytometer (BD Biosciences) and the data were analyzed through the CellQuest Pro v6.0 software (BD Biosciences).

 © 2021 The Authors

Terminal deoxynucleotidyl transferase dUTP nick end labeling (TUNEL) assay

The HeLa CCL2 cells treated with either control luciferase (shGL) or shβ-catenin lentiviruses for 1 day and then selected with 4 μg/ml of puromycin for 1 day. Cells were harvested at 24, 48, 72, and 96 h after puromycin selection and subjected to TUNEL assay by using In Situ Cell Death Detection Kit, Fluorescein (Roche, Indianapolis, IN) according to manufacturer's instructions. Briefly, cells were fixed with 4% paraformaldehyde for 30 min at room temperature, permeabilized with 0.1% Triton X-100 in 0.1% sodium citrate for 10 min at RT, and the resulting cells were labeled with TUNEL reaction mixture for 1 h at 37°C dark. DNA was stained, coverslips were mounted on the glass slides, and fluorescence signals were observed/photographed under a fluorescence microscopy as described in immunofluorescence assay section.

Rho activation assay

HeLa CCL2 cells either infected with lentiviruses or transfected with DNA constructs as indicated in Figs 5I and 6G, respectively, were lysed with lysis buffer (50 mM Tris pH 7.5, 10 mM $MgCl_2$, 0.5 M NaCl, and 2% Igepal) as described in manufacturer's protocol (BK036; Rho Activation Assay Biochem Kit; Cytoskeleton, Los Angeles, CA). The resulting cell lysates were applied to Rho Activation Assay Biochem Kit (Cytoskeleton) according to manufacturer's instructions. Briefly, cell lysates (0.5–1 mg) were incubated with 20 μg of rhotekin-RBD beads for 1 h at 4°C. Beads were then precipitated by centrifugation at 5000 × *g* for 1 min at 4°C and washed with wash buffer (25 mM Tris pH 7.5, 30 mM $MgCl_2$, 40 mM NaCl) 2 times. The resulting beads were subjected to SDS–PAGE followed by immunoblotting with anti-Rho antibody.

TopFlash/FopFlash luciferase assay Luciferase reporter assay

To determine β-catenin-dependent transcriptional activation during mitosis, we performed TopFlash (eight copies of the TCF/LEF binding sites)/FopFlash (a mutant of TCF/LEF binding sites) luciferase assay. HEK293T cells were co-transfected with the indicated Firefly luciferase reporter plasmid, either SuperTopFlash or FopFlash reporter plasmids (gifts of Randall T. Moon, University of Washington, Seattle, WA), and control pRL-TK Renilla luciferase reporter plasmid (Promega, Madison, WI). 24 h after transfection, the medium was replaced with serum-free medium containing DMSO or nocodazole (200 ng/ml), and the cells were incubated for an additional 12 h, and then, the cells were treated with either control or Wnt3a CM for 6 h. The resulting cells were harvested and subjected to luciferase assay using a Dual Luciferase Assay Kit (Promega). Luciferase activities were measured by using 2030 Multilabel Reader VICTOR^{TM} ×2 (PerkinElmer Life and Analytical Science, Boston, MA).

Midbody isolation

Midbody isolation was carried out as described previously (Mullins & McIntosh, 1982) with brief modifications. Briefly, cells harvested with centrifugation at 200 *g* for 3 min were gently resuspended in 25 vol. hypotonic swelling solution {1 M hexylene glycol, 20 μM $MgCl_2$, 2 mM PIPES (pH 7.2)} at RT. Resulting cells were centrifuged at 200 g for 3 min. Pellets were vigorously resuspended by vortexing in 50 vol. lysis solution {(1 M hexylene glycol, 1 mM EGTA, 1% NP-40, 2 mM PIPES (pH 7.2)} for 30 s. at 37°C. Isolated midbodies were stabilized by chilling on ice. Add 0.3 vol. stabilizing solution {(1 M hexylene glycol, 30 mM 2-(*N*-morpholino)ethane sulfonic acid (MES) (pH 6.3)}. Lysates were centrifuged at 250 *g* for 10 min, and resulting supernatants were applied to glycerol cushion {(40% glycerol (w/v) in 50 mM MES (pH 6.3)}. Midbody pellets were isolated by centrifugation for 40 min at 2,800 *g*. Pellets were washed with 50 mM MES buffer (pH 6.3) twice.

Statistical analysis

Statistical analyses were performed using Excel (Microsoft) for unpaired two-tailed *t*-test of Figs 5D, 6H and 7B, Appendix Figs S6A, S7E, S9B, D and G, and SigmaPlot 13.0 (Systat Software, San Jose, CA) for one-way ANOVA of Fig 5C, Appendix Figs S5B and S10B.

Data availability

No data were deposited in a public database.

Expanded View for this article is available online.

Acknowledgements
We thank Kyung S. Lee, Kunsoo Rhee, Sean B. Lee, Michael B. Yaffe, Randall T. Moon, Eric R. Fearon, W. James Nelson, Adrienne Cox, Phillip A. Sharp, and Sheila A. Stewart for reagents. This work was supported by the National Research Foundation of Korea (NRF) grant funded by the Korean government (MSIT) (NRF-2021R1A2C1004854), (NRF-2021R1A2C3004965), R&D Convergence Program (CAP-16-03-KRIBB) of National Research Council of Science & Technology (NST) of Republic of Korea, and KRIBB Research Initiative Program.

Author contributions
KHL and JEY designed the experiments; KHL, JEY, SOK, NKS, HCM, JH, and, JAH performed the experiments; KHL, JEY, SOK, JTH, YTK, and BYK analyzed the data; KHL and JEY wrote the paper.

Conflict of interest
The authors declare that they have no conflicts of interest with the contents of this article.

References

Aoki K, Aoki M, Sugai M, Harada N, Miyoshi H, Tsukamoto T, Mizoshita T, Tatematsu M, Seno H, Chiba T *et al* (2007) Chromosomal instability by beta-catenin/TCF transcription in APC or beta-catenin mutant cells. *Oncogene* 26: 3511 – 3520

Bahmanyar S, Kaplan DD, Deluca JG, Giddings Jr TH, O'Toole ET, Winey M, Salmon ED, Casey PJ, Nelson WJ, Barth AI (2008) β-Catenin is a Nek2 substrate involved in centrosome separation. *Genes Dev* 22: 91 – 105

Barr FA, Silljé HH, Nigg EA (2004) Polo-like kinases and the orchestration of cell division. *Nat Rev Mol Cell Biol* 5: 429 – 440

Barrallo-Gimeno A, Nieto MA (2005) The Snail genes as inducers of cell movement and survival: implications in development and cancer. *Development* 132: 3151 – 3161

© 2021 The Authors

Behrens J (2005) The role of the Wnt signalling pathway in colorectal tumorigenesis. *Biochem Soc Trans* 33: 672 – 675

Behrens J, von Kries JP, Kühl M, Bruhn L, Wedlich D, Grosschedl R, Birchmeier W (1996) Functional interaction of beta-catenin with the transcription factor LEF-1. *Nature* 382: 638 – 642

Bement WM, Benink HA, von Dassow G (2005) A microtubule-dependent zone of active RhoA during cleavage plane specification. *J Cell Biol* 170: 91 – 101

Bienz M, Clevers H (2000) Linking colorectal cancer to Wnt signaling. *Cell* 103: 311 – 320

Birkenfeld J, Nalbant P, Bohl BP, Pertz O, Hahn KM, Bokoch GM (2007) GEF-H1 modulates localized RhoA activation during cytokinesis under the control of mitotic kinases. *Dev Cell* 12: 699 – 712

Brennan IM, Peters U, Kapoor TM, Straight AF (2007) Polo-like kinase controls vertebrate spindle elongation and cytokinesis. *PLoS One* 2: e409

Brunner E, Peter O, Schweizer L, Basler K (1997) Pangolin encodes a Lef-1 homologue that acts downstream of Armadillo to transduce the Wingless signal in *Drosophila*. *Nature* 385: 829 – 833

Burkard ME, Randall CL, Larochelle S, Zhang C, Shokat KM, Fisher RP, Jallepalli PV (2007) Chemical genetics reveals the requirement for Polo-like kinase 1 activity in positioning RhoA and triggering cytokinesis in human cells. *Proc Natl Acad Sci USA* 104: 4383 – 4388

Conacci-Sorrell M, Simcha I, Ben-Yedidia T, Blechman J, Savagner P, Ben-Zeev A (2003) Autoregulation of E-cadherin expression by cadherin-cadherin interactions: the roles of β-catenin signaling, Slug, and MAPK. *J Cell Biol* 163: 847 – 857

Davidson G, Shen J, Huang YL, Su Y, Karaulanov E, Bartscherer K, Hassler C, Stannek P, Boutros M, Niehrs C (2009) Cell cycle control of wnt receptor activation. *Dev Cell* 17: 788 – 799

Dierick H, Bejsovec A (1999) Cellular mechanisms of wingless/Wnt signal transduction. *Curr Top Dev Biol* 43: 153 – 190

Duijf PH, Schultz N, Benezra R (2013) Cancer cells preferentially lose small chromosomes. *Int J Cancer* 132: 2316 – 2326

Eastman Q, Grosschedl R (1999) Regulation of LEF-1/TCF transcription factors by Wnt and other signals. *Curr Opin Cell Biol* 11: 233 – 240

Eggert US, Mitchison TJ, Field CM (2006) Animal cytokinesis: from parts list to mechanisms. *Annu Rev Biochem* 75: 543 – 566

Elbashir SM, Harborth J, Lendeckel W, Yalcin A, Weber K, Tuschl T (2001) Duplexes of 21-nucleotide RNAs mediate RNA interference in cultured mammalian cells. *Nature* 411: 494 – 498

Elia AE, Rellos P, Haire LF, Chao JW, Ivins FJ, Hoepker K, Mohammad D, Cantley LC, Smerdon SJ, Yaffe MB (2003) The molecular basis for phosphodependent substrate targeting and regulation of Plks by the Polo-box domain. *Cell* 115: 83 – 95

Fang D, Hawke D, Zheng Y, Xia Y, Meisenhelder J, Nika H, Mills GB, Kobayashi R, Hunter T, Lu Z (2007) Phosphorylation of beta-catenin by AKT promotes beta-catenin transcriptional activity. *J Biol Chem* 282: 11221 – 11229

Fededa JP, Gerlich DW (2012) Molecular control of animal cell cytokinesis. *Nat Cell Biol* 14: 440 – 447

Green RA, Paluch E, Oegema K (2012) Cytokinesis in animal cells. *Annu Rev Cell Dev Biol* 28: 29 – 58

Hadjihannas MV, Brückner M, Jerchow B, Birchmeier W, Dietmaier W, Behrens J (2006) Aberrant Wnt/beta-catenin signaling can induce chromosomal instability in colon cancer. *Proc Natl Acad Sci USA* 103: 10747 – 10752

Heuberger J, Birchmeier W (2010) Interplay of cadherin-mediated cell adhesion and canonical Wnt signaling. *Cold Spring Harb Perspect Biol* 2: a002915

Huber O, Korn R, McLaughlin J, Ohsugi M, Herrmann BG, Kemler R (1996) Nuclear localization of beta-catenin by interaction with transcription factor LEF-1. *Mech Dev* 59: 3 – 10

Kaplan DD, Meigs TE, Kelly P, Casey PJ (2004) Identification of a role for β-catenin in the establishment of a bipolar mitotic spindle. *J Biol Chem* 279: 10829 – 10832

Kikuchi K, Niikura Y, Kitagawa K, Kikuchi A (2010) Dishevelled, a Wnt signalling component, is involved in mitotic progression in cooperation with Plk1. *EMBO J* 29: 3470 – 3483

Kim S, Jeong S (2019) Mutation hotspots in the β-catenin gene: lessons from the human cancer genome databases. *Mol Cells* 42: 8 – 16

Kishi K, van Vugt MA, Okamoto K, Hayashi Y, Yaffe MB (2009) Functional dynamics of Polo-like kinase1 at the centrosome. *Mol Cell Biol* 29: 3134 – 3150

Kyun M-L, Kim S-O, Lee HG, Hwang J-A, Hwang J, Soung N-K, Cha-Molstad H, Lee S, Kwon YT, Kim BY *et al* (2020) Wnt3a stimulation promotes primary ciliogenesis through β-catenin phosphorylation-induced reorganization of centriolar satellites. *Cell Rep* 30: 1447 – 1462

Lee KH, Hwang J-A, Kim S-O, Kim JH, Shin SC, Kim EE, Lee KS, Rhee K, Jeon BH, Bang JK *et al* (2018) Phosphorylation of human enhancer filamentation 1 (HEF1) stimulates interaction with Polo-like kinase 1 leading to HEF1 localization to focal adhesions. *J Biol Chem* 293: 847 – 862

Lee KH, Johmura Y, Yu LR, Park JE, Gao Y, Bang JK, Zhou M, Veenstra TD, Kim BY, Lee KS (2012) Identification of a novel Wnt5a-CK1ε-Dvl2-Plk1-mediated primary cilia disassembly pathway. *EMBO J* 31: 3104 – 3117

Lee KS, Yuan YL, Kuriyama R, Erikson RL (1995) Plk is an M-phase-specific protein kinase and interacts with a kinesin-like protein, CHO1/MKLP-1. *Mol Cell Biol* 15: 7143 – 7151

Lee U, Kim SO, Hwang JA, Jang JH, Son S, Ryoo IJ, Ahn JS, Kim BY, Lee KH (2017) The fungal metabolite brefeldin A inhibits Dvl2-Plk1-dependent primary cilium disassembly. *Mol Cells* 40: 401 – 409

Lens SMA, Medema RH (2019) Cytokinesis defects and cancer. *Nat Rev Cancer* 19: 32 – 45

Liu C, Kato Y, Zhang Z, Do VM, Yankner BA, He X (1999) Beta-Trcp couples beta-catenin phosphorylation-degradation and regulates Xenopus axis formation. *Proc Natl Acad Sci USA* 96: 6273 – 6278

Liu C, Li Y, Semenov M, Han C, Baeg GH, Tan Y, Zhang Z, Lin X, He X (2002) Control of beta-catenin phosphorylation/degradation by a dual-kinase mechanism. *Cell* 108: 837 – 847

Mbom BC, Nelson WJ, Barth A (2013) β-catenin at the centrosome: discrete pools of β-catenin communicate during mitosis and may co-ordinate centrosome functions and cell cycle progression. *BioEssays* 35: 804 – 809

Molenaar M, van de Wetering M, Oosterwegel M, Peterson-Maduro J, Godsave S, Korinek V, Roose J, Destrée O, Clevers H (1996) XTCF-3 transcription factor mediates beta-catenin-induced axis formation in Xenopus embryos. *Cell* 86: 391 – 399

Moon RT, Bowerman B, Boutros M, Perrimon N (2002) The promise and perils of Wnt signaling through β-catenin. *Science* 296: 1644 – 1646

Mullins JM, McIntosh JR (1982) Isolation and initial characterization of the mammalian midbody. *J Cell Biol* 94: 654 – 661

Nakajima H, Toyoshima-Morimoto F, Taniguchi E, Nishida E (2003) Identification of a consensus motif for Plk (Polo-like kinase) phosphorylation reveals Myt1 as a Plk1 substrate. *J Biol Chem* 278: 25277 – 25280

Nelson WJ, Nusse R (2004) Convergence of Wnt, β-catenin, and cadherin pathways. *Science* 303: 1483 – 1487

 © 2021 The Authors

Niiya F, Tatsumoto T, Lee KS, Miki T (2006) Phosphorylation of the cytokinesis regulator ECT2 at G2/M phase stimulates association of the mitotic kinase Plk1 and accumulation of GTP-bound RhoA. *Oncogene* 25: 827 – 837

Nishimura Y, Yonemura S (2006) Centralspindlin regulates ECT2 and RhoA accumulation at the equatorial cortex during cytokinesis. *J Cell Sci* 119: 104 – 114

Odell GM, Foe VE (2008) An agent-based model contrasts opposite effects of dynamic and stable microtubules on cleavage furrow positioning. *J Cell Biol* 183: 471 – 483

Ozawa M, Baribault H, Kemler R (1989) The cytoplasmic domain of the cell adhesion molecule uvomorulin associates with three independent proteins structurally related in different species. *EMBO J* 8: 1711 – 1717

Peifer M, Polakis P (2000) Wnt signaling in oncogenesis and embryogenesis—A look outside the nucleus. *Science* 287: 1606 – 1609

Petronczki M, Glotzer M, Kraut N, Peters JM (2007) Polo-like kinase 1 triggers the initiation of cytokinesis in human cells by promoting recruitment of the RhoGEF Ect2 to the central spindle. *Dev Cell* 12: 713 – 725

Petronczki M, Lénárt P, Peters JM (2008) Polo on the rise – from mitotic entry to cytokinesis with Plk1. *Dev Cell* 14: 646 – 659

Riggleman B, Schedl P, Wieschaus E (1990) Spatial expression of the *Drosophila* segment polarity gene armadillo is posttranscriptionally regulated by wingless. *Cell* 63: 549 – 560

Roura S, Miravet S, Piedra J, García de Herreros A, Duñach M (1999) Regulation of E-cadherin/Catenin association by tyrosine phosphorylation. *J Biol Chem* 274: 36734 – 36740

Santamaria A, Neef R, Eberspächer U, Eis K, Husemann M, Mumberg D, Prechtl S, Schulze V, Siemeister G, Wortmann L *et al* (2007) Use of the novel Plk1 inhibitor ZK-thiazolidinone to elucidate functions of Plk1 in early and late stages of mitosis. *Mol Biol Cell* 18: 4024 – 4036

Schlesinger A, Shelton CA, Maloof JN, Meneghini M, Bowerman B (1999) Wnt pathway components orient a mitotic spindle in the early *Caenorhabditis elegans* embryo without requiring gene transcription in the responding cell. *Genes Dev* 13: 2028 – 2038

Su KC, Takaki T, Petronczki M (2011) Targeting of the RhoGEF Ect2 to the equatorial membrane controls cleavage furrow formation during cytokinesis. *Dev Cell* 21: 1104 – 1115

Valenta T, Hausmann G, Basler K (2012) The many faces and functions of β-catenin. *EMBO J* 31: 2714 – 2736

van de Wetering M, Cavallo R, Dooijes D, van Beest M, van Es J, Loureiro J, Ypma A, Hursh D, Jones T, Bejsovec A *et al* (1997) Armadillo coactivates transcription driven by the product of the *Drosophila* segment polarity gene dTCF. *Cell* 88: 789 – 799

Walston T, Tuskey C, Edgar L, Hawkins N, Ellis G, Bowerman B, Wood W, Hardin J (2004) Multiple Wnt signaling pathways converge to orient the mitotic spindle in early *C. elegans* embryos. *Dev Cell* 7: 831 – 841

Weaver BA, Cleveland DW (2007) Aneuploidy: instigator and inhibitor of tumorigenesis. *Cancer Res* 67: 10103 – 10105

Wieschaus E, Riggleman R (1987) Autonomous requirements for the segment polarity gene armadillo during *Drosophila* embryogenesis. *Cell* 49: 177 – 184

Winston JT, Strack P, Beer-Romero P, Chu CY, Elledge SJ, Harper JW (1999) The SCFbeta-TRCP-ubiquitin ligase complex associates specifically with phosphorylated destruction motifs in IkappaBalpha and beta-catenin and stimulates IkappaBalpha ubiquitination in vitro. *Genes Dev* 13: 270 – 283

Wolfe BA, Takaki T, Petronczki M, Glotzer M (2009) Polo-like kinase 1 directs assembly of the HsCyk-4 RhoGAP/Ect2 RhoGEF complex to initiate cleavage furrow formation. *PLoS Biol* 7: e1000110

Wu G, He X (2006) Threonine 41 in beta-catenin serves as a key phosphorylation relay residue in beta-catenin degradation. *Biochemistry* 45: 5319 – 5323

Yang J, Mani SA, Donaher JL, Ramaswamy S, Itzykson RA, Come C, Savagner P, Gitelman I, Richardson A, Weinberg RA (2004) Twist, a master regulator of morphogenesis, plays an essential role in tumor metastasis. *Cell* 117: 927 – 939

Yuce O, Piekny A, Glotzer M (2005) An ECT2-centralspindlin complex regulates the localization and function of RhoA. *J Cell Biol* 170: 571 – 582

Yun S-M, Moulaei T, Lim D, Bang JK, Park J-E, Shenoy SR, Liu FA, Kang YH, Liao C, Soung N-K *et al* (2009) Structural and functional analyses of minimal phosphopeptides targeting the polo-box domain of polo-like kinase 1. *Nat Struct Mol Biol* 16: 876 – 882

Zhao WM, Fang G (2005) Anillin is a substrate of anaphase-promoting complex/cyclosome (APC/C) that controls spatial contractility of myosin during late cytokinesis. *J Biol Chem* 280: 33516 – 33524

License: This is an open access article under the terms of the Creative Commons Attribution-NonCommercial-NoDerivs License, which permits use and distribution in any medium, provided the original work is properly cited, the use is non-commercial and no modifications or adaptations are made.